European Journal of Medicinal Chemistry 80 (2014) 543–561

Contents lists available at ScienceDirect

European Journal of Medicinal Chemistry

journal homepage: http://www.elsevier.com/locate/ejmech

Original article

Donepezil + propargylamine + 8-hydroxyquinoline hybrids as new multifunctional metal-chelators, ChE and MAO inhibitors for the potential treatment of Alzheimer's disease

Li Wang [a,1], Gerard Esteban [b,1], Masaki Ojima [a], Oscar M. Bautista-Aguilera [c], Tsutomu Inokuchi [a,*], Ignacio Moraleda [d], Isabel Iriepa [d], Abdelouahid Samadi [c], Moussa B.H. Youdim [e], Alejandro Romero [f], Elena Soriano [g], Raquel Herrero [h], Ana Patricia Fernández Fernández [h], Ricardo-Martínez-Murillo [h], José Marco-Contelles [c,*], Mercedes Unzeta [b,*]

[a] *Division of Chemistry and Biotechnology, Graduate School of Natural Science and Technology, Okayama University, 3.1.1 Tsushima-Naka, Kita-ku, Okayama 700-8530, Japan*
[b] *Departament de Bioquímica i Biologia Molecular, Facultat de Medicina, Institut de Neurociències, Universitat Autònoma de Barcelona, 08193 Bellaterra, Barcelona, Spain*
[c] *Laboratorio de Química Médica (IQOG, CSIC), C/Juan de la Cierva 3, 28006 Madrid, Spain*
[d] *Departamento de Química Orgánica y Química Inorgánica, Universidad de Alcalá, Ctra. Madrid-Barcelona, Km. 33,6, 28871 Alcalá de Henares, Madrid, Spain*
[e] *Eve Topf Centers of Excellence for Neurodegenerative Diseases Research and Department of Pharmacology, Rappaport Family Research Institute, Technion-Faculty of Medicine, Haifa 31096, Israel*
[f] *Departamento de Toxicología y Farmacología, Facultad de Veterinaria, Universidad Complutense de Madrid, 28040 Madrid, Spain*
[g] *SEPCO, IQOG (CSIC), Juan de la Cierva, 3, 28006 Madrid, Spain*
[h] *Neurovascular Research Group, Department of Molecular, Cellular and Developmental Neurobiology, Instituto Cajal (CSIC) Av. Doctor Arce 37, 28002 Madrid, Spain*

ARTICLE INFO

Article history:
Received 10 February 2014
Received in revised form
24 April 2014
Accepted 26 April 2014
Available online 29 April 2014

Keywords:
Donepezil + Propargylamine + 8-Hydroxyquinoline hybrids
Multifunctional drugs
Fe/Cu/Zn chelators
ChE and MAO inhibitors
In vivo scopolamine-induced long-term memory deficit
Alzheimer's disease

ABSTRACT

The synthesis, biochemical evaluation, ADMET, toxicity and molecular modeling of novel multi-target-directed **D**onepezil + **P**ropargylamine + 8-**H**ydroxyquinoline (**DPH**) hybrids **1**–**7** for the potential prevention and treatment of Alzheimer's disease is described. The most interesting derivative was racemic α-aminotrile4-(1-benzylpiperidin-4-yl)-2-(((8-hydroxyquinolin-5-yl)methyl)(prop-2-yn-1-yl)amino) butanenitrile (**DPH6**) [MAO A (IC_{50} = 6.2 ± 0.7 μM; MAO B (IC_{50} = 10.2 ± 0.9 μM); AChE (IC_{50} = 1.8 ± 0.1 μM); BuChE (IC_{50} = 1.6 ± 0.25 μM)], an irreversible MAO A/B inhibitor and mixed-type AChE inhibitor with metal-chelating properties. According to docking studies, both **DPH6** enantiomers interact simultaneously with the catalytic and peripheral site of *Ee*AChE through a linker of appropriate length, supporting the observed mixed-type AChE inhibition. Both enantiomers exhibited a relatively similar position of both hydroxyquinoline and benzyl moieties with the rest of the molecule easily accommodated in the relatively large cavity of MAO A. For MAO B, the quinoline system was hosted at the cavity entrance whereas for MAO A this system occupied the substrate cavity. In this disposition the quinoline moiety interacted directly with the FAD aromatic ring. Very similar binding affinity values were also observed for both enantiomers with ChE and MAO enzymes. **DPH** derivatives exhibited moderate to good ADMET properties and brain penetration capacity for CNS activity. **DPH6** was less toxic than donepezil at high concentrations; while at low concentrations both displayed a similar cell viability profile. Finally, in a passive avoidance task, the antiamnesic effect of **DPH6** was tested on mice with experimentally induced amnesia. DPH6 was capable to significantly decrease scopolamine-induced learning deficits in healthy adult mice.

* Corresponding authors.
E-mail addresses: Mercedes.Unzeta@uab.cat, mercedes.unzeta@uab.es (M. Unzeta).
[1] G.E. and L.W. have equally contributed to this work.

http://dx.doi.org/10.1016/j.ejmech.2014.04.078
0223-5234/

1. Introduction

Alzheimer's disease (AD) is an age-related neurodegenerative process characterized by progressive memory loss and other cognitive impairments [1]. Although its etiology has not yet been elucidated, β-amyloid (Aβ) deposits [2], τ-protein phosphorylation, oxidative stress [3] and deficits of acetylcholine (ACh) [4] are considered to play significant roles in the pathophysiology of AD [5]. Consequently, AD patients have been treated with acetylcholinesterase inhibitors (AChEI) [6] with limited therapeutic success. This might be due to the multifactorial nature of AD, a fact that has prompted the hunt for new Multi-Target-Directed Ligands (MTDL), based on the "one molecule, multiple target" paradigm [7]. Thus, in this context, multifunctional molecules able to simultaneously bind both cholinesterases and monoamineoxidases have been investigated [8,9].

Monoamine oxidase (MAO; EC 1.4.3.4) is an important target to be considered for the treatment of AD, as it catalyzes the oxidative deamination of a variety of biogenic and xenobiotic amines with the concomitant production of hydrogen peroxide, a key intermediate *via* Fenton reaction in the production of toxic radical oxygenated species implicated in the progress of AD. MAO is a FAD (Flavin-Adenine Dinucleotide)-containing enzyme bound to mitochondrial outer membranes of neuronal, glial and other cells [10]. MAO exists as two isoenzymes, MAO A/B, displaying different substrate specificity, sensitivity to inhibitors, and amino acid sequences. While MAO A preferentially oxidizes neurotransmitters norepinephrine and serotonin and it is selectively inhibited by clorgyline, MAO B preferentially deaminates β-phenylethylamine and it is irreversibly inhibited by l-deprenyl [11]. X-ray crystal structures of rat MAO A [12] and human MAO B have been reported [13].

Taken these facts into account, we previously reported the synthesis and biological evaluation of new multifunctional MAO/ChE inhibitor ASS234 [8,9] (Chart 1) by combining the N-benzylpiperidine and the N-propargylamine moieties present in donepezil, and PF9601N [14], ChE and MAO inhibitors, respectively.

In this work we report the design, synthesis, biochemical evaluation and molecular modeling of Donepezil + Propargylamine + 8-Hydroxyquinoline (DPH) hybrids 1–7 and the identification of the racemic α-aminonitrile 4-(1-benzylpiperidin-4-yl)-2-(((8-hydroxyquinolin-5-yl)methyl)(prop-2-yn-1-yl)amino)butanenitrile (DPH6) (Table 1), as a multifunctional lead molecule for the potential treatment of AD. These hybrids are the result of the juxtaposition of donepezil, a selective AChE inhibitor currently used in the pharmacological treatment of AD, and M30 (Chart 1), a potent brain selective MAO A/B inhibitor and neuroprotective biometal-chelator [15]. HLA20A (Chart 1) is a novel pro-chelator with improved cytotoxicity exhibiting poor affinity for metal ions while not being activated to an active chelator by binding and inhibiting AChE, being able to modulate amyloid precursor protein (APP) and to reduce Aβ aggregation [16].

2. Results and discussion

2.1. Chemistry

DPHs 1–7 were prepared as shown in Schemes 1–5 by using reductive amination of suitable and different carbaldehydes bearing the *N*-benzylpiperidine nucleus and propargylamine, followed by *N*-alkylation with easily available 5-(chloromethyl)quinolin-8-ol (**8**) [17] (**Experimental Part**).

In the reductive amination leading to the intermediates for the preparation of **DPH3**, **DPH5** and **DPH7**, we have also isolated and characterized the unexpected α-aminonitriles **11**, **16** and **21** that have been similarly transformed into racemic α-aminonitriles **DPH2**, **DPH4** and **DPH6**. In order to confirm the structure of **DPH6**, an alternative, unequivocal synthesis of α-aminonitrile **21** has been achieved from aldehyde **19** *via* Strecker-type reaction (Scheme 5), followed by standard *N*-alkylation as shown above.

All new compounds showed analytical and spectroscopic data, in good agreement with their structure (**Experimental Part**).

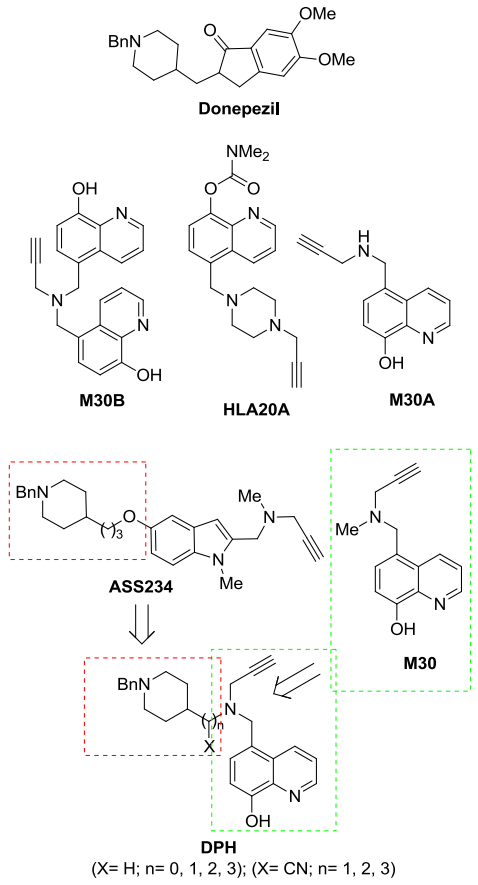

Chart 1. General structure of donepezil, M30, M30A, M30B, HLA20A, ASS234, and the new multifunctional ChE/MAO DPH inhibitors described in this work.

2.2. Pharmacological evaluation

2.2.1. Cholinesterase inhibition

The in vitro activity of DPHs 1–7 derivatives as *Ee*AChE and eqBuChE inhibitors was assessed using the Ellman's method [18] (Table 1).

From these data some interesting structure–activity relationships (SAR) were obtained. DPH1, bearing no methyl in the linker connecting the N-benzyl-piperidin-4′-yl residue to the N-propargyl core, was inactive. In comparison, DPHs 2–7 derivatives were non-selective moderate ChE inhibitors, DPH6 ($n = 3$ in the linker) exhibiting the most potent profile [*Ee*AChE ($IC_{50} = 1.8 \pm 0.1$ μM); eqBuChE ($IC_{50} = 1.6 \pm 0.25$ μM)]. Regarding tertiary amines DPHs 3, 5 and 7, activity at inhibiting both cholinesterases gradually increased from DPH3 ($n = 1$) to DPH7 ($n = 3$), which displayed the most active profile [*Ee*AChE ($IC_{50} = 2.7 \pm 0.4$ μM); eqBuChE ($IC_{50} = 4.5 \pm 0.3$ μM)]. A similar trend was detected with the α-aminonitrile series (DPHs 2, 4 and 6), with DPH6 ($n = 3$) as the most potent anticholinesterasic compound. Generally, for equivalent linker length, α-aminonitriles derivatives proved to be more potent than amines at inhibiting both enzymes, with the exception of

Table 1
Dose-response values [IC_{50} (μM)] of membrane-bound MAO A and MAO B from rat liver, electric eel AChE (*Ee*AChE) and equine BuChE (eqBuChE) with DPH derivatives and standard inhibitors.

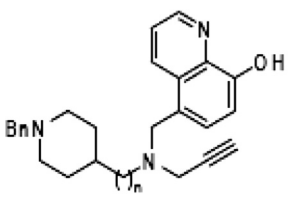

1 n= 0
3 n= 1
5 n= 2
7 n= 3

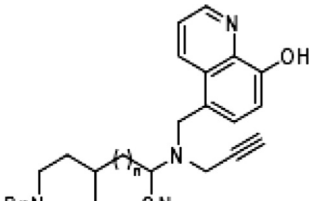

2 n= 0
4 n= 1
6 n= 2

DPH	EeAChE[a]	eqBuChE[a]	SI[c]	ratMAO A[b]	ratMAO B[b]	SI[d]
1	≥100	≥100	–	≥100	≥100	≥1
2	14.5 ± 3.7	13.5 ± 1.8	0.92	22.1 ± 0.7	39.5 ± 1.4	1.7
3	17.0 ± 4.7	12.8 ± 1.4	0.75	85.4 ± 3.7	19.4 ± 3.2	0.22
4	5.5 ± 0.5	6.1 ± 0.6	1.1	9.7 ± 1.5	12.4 ± 2.5	1.2
5	5.0 ± 0.8	14.5 ± 3.6	2.8	≥100	50.1 ± 5.0	≥0.5
6	1.8 ± 0.1	1.6 ± 0.2	0.92	6.2 ± 0.7	10.2 ± 0.9	1.7
7	2.7 ± 0.4	4.5 ± 0.3	1.6	≥100	34.5 ± 3.5	≥0.34
Donepezil	0.0067 ± 0.0004	7.4 ± 0.1	1100	850 ± 13	15 ± 2.2	0.02
M-30 [15] 113.9 ± 14.05	≥100	–	0.037 ± 0.02	0.057 ± 0.02	1.5	
***l*-Deprenyl** [14] ≥500	≥500	–	3	0.02	0.0067	
Clorgyline [22]	≥500	≥500	–	0.03	8	267

end = values not determined.
Values are expressed as mean ± standard error of the mean of at least three different experiments in quadruplicate.
[a] 20-min pre-incubation.
[b] 30-min pre-incubation.
[c] eqBuChE selectivity index = IC_{50} (eqBuChE)/IC_{50} (*Ee*AChE).
[d] MAO B selectivity index = IC_{50} (MAO B)/IC_{50} (MAO A).

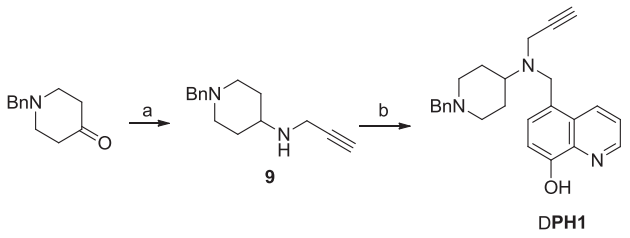

Scheme 1. Synthesis of **DPH1**. Reagents and conditions: (a) i. 1-Benzyl-4-piperidone, MeOH, TFA; ii. $NaBH_3CN$ (31%); (b) 5-(chloromethyl) quinolin-8-ol (8), DCM, Et_3N (33%).

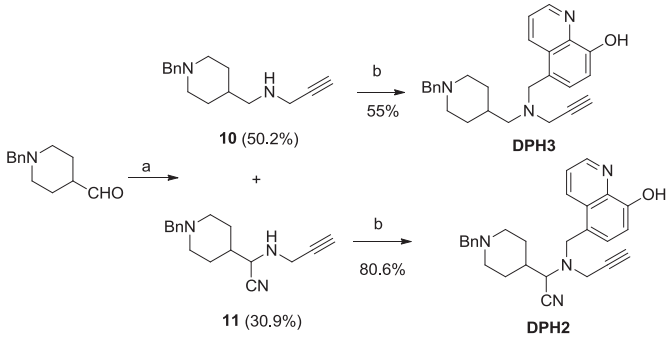

Scheme 2. Synthesis of **DPH2** and **DPH3**. Reagents and conditions: (a) i. Propargylamine, MeOH, TFA; ii, $NaBH_3CN$; (b) 5-(chloromethyl) quinolin-8-ol (8), DCM, Et_3N.

DPH4 and DPH5 exhibiting similar antiacetylcholinesterase activity. In comparison to donepezil, DPH6 was significantly less active *Ee*AChE inhibitor, but more potent at inhibiting eqBuChE (4.5-fold). Moreover, DPH6 was 64-fold more potent inhibiting both cholinesterases than M30 (Chart 1), inactive on this enzyme.

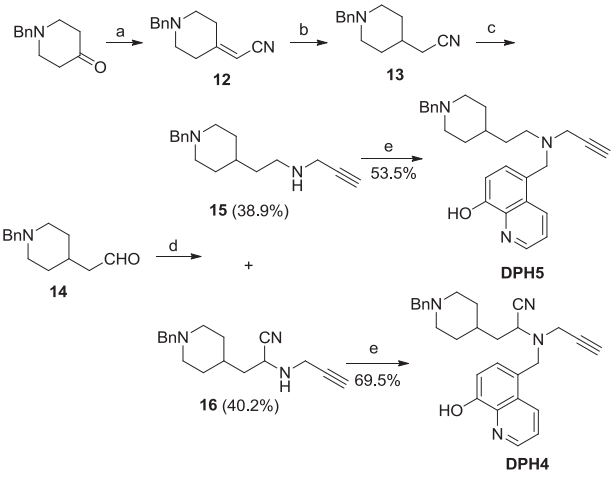

Scheme 3. Synthesis of **DPH4** and **DPH5**. Reagents and conditions: (a) Diethyl(cyanomethyl)phosphonate, K_2CO_3, THF (99%); (b) I_2, Mg, MeOH (74%); (c) DIBALH, THF, -78 °C (27%); (d) i. Propargylamine, MeOH, TFA; ii. $NaBH_3CN$; (e) 5-(chloromethyl) quinolin-8-ol (8), DCM, Et_3N.

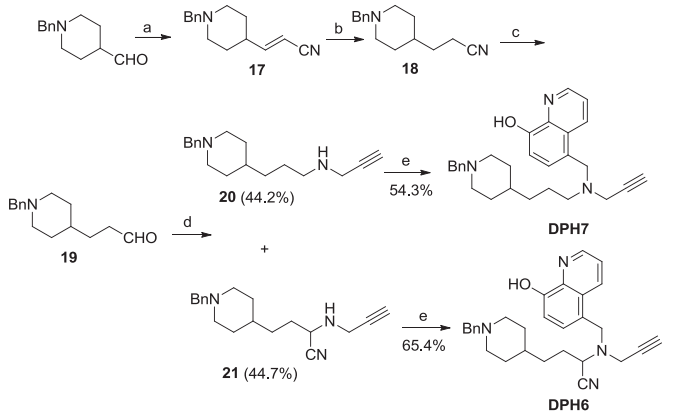

Scheme 4. Synthesis of **DPH6** and **DPH7**. Reagents and conditions: (a) Diethyl(cyanomethyl) phosphonate, K_2CO_3, THF (33%); (b) I_2, Mg, MeOH (99%); (c) DIBALH, THF, -78 °C (28); (d) i. Propargylamine, MeOH, TFA; ii. $NaBH_3CN$; (e) 5-(chloromethyl) quinolin-8-ol (8), DCM, Et_3N.

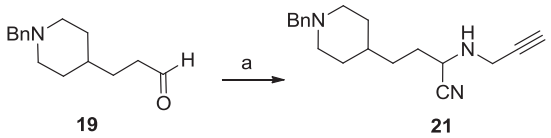

Scheme 5. Alternative synthesis of compound **21**. Reagents and conditions: (a) Propargylamine, TMSCN, MWI, 125 °C, 10 min (60%)

To determine the type of AChE inhibition exerted by DPH6, Lineweaver–Burk reciprocal plots were obtained (Fig. 1). Increasing slopes (decreasing V_{max}) and intercepts (increasing K_m) with higher inhibitory concentration were determined suggesting a mixed type inhibition. Reversible inhibition constant (k_i) of 1.21 ± 0.25 μM was estimated from the slopes of double reciprocal plots versus DPH6 concentrations.

2.2.2. Monoamine oxidase inhibition

In order to assess their multipotent profile, the inhibitory capacity of DPHs 1–7 as dual MAO A and MAO B inhibitors was evaluated using [^{14}C]-5HT and [^{14}C]-phenylethylamine as substrates, respectively [19]. As shown in Table 1, most of DPH derivatives poorly inhibited MAO, except DPH 4 and DPH6 that showed moderate, almost equipotent inhibitory activity on both enzyme isoforms. Once more, DPH6 revealed the most potent profile at inhibiting both monoamine oxidase isoforms [MAO A (IC_{50} = 6.2 ± 0.7 μM; MAO B (IC_{50} = 10.2 ± 0.9 μM)]. Compared to M30 (Chart 1) [15], DPH6 was 166-fold and 179-fold less potent inhibiting MAO A and MAO B, respectively. Yet, DPH6 was 138-fold more active than donepezil, showing equipotency at inhibiting MAO A and MAO B, respectively. The previously mentioned SAR also applied: for similar linker length, α-aminonitriles were more potent inhibitors than their corresponding amines versus both isoenzymes, with the exception of DPH2 as MAO B inhibitor. From dose–response curves (IC_{50}), DPH6 showed a non-selective MAO inhibition in comparison to standard selective MAO B and MAO A inhibitors l-deprenyl [14] and clorgyline [20], respectively.

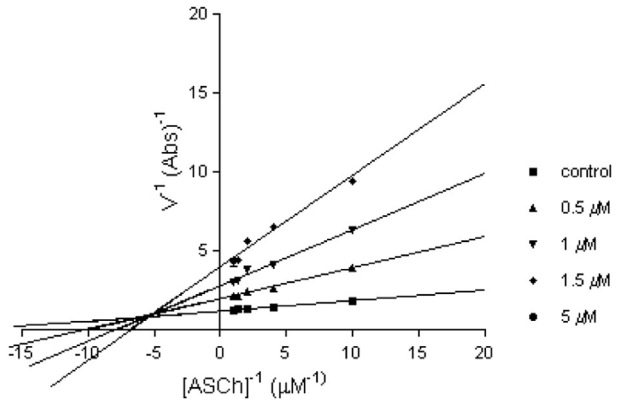

Fig. 1. Steady-state inhibition of *Ee*AChE hydrolysis of acetylthiocholine (ASCh) by **DHP6** (0–5 μM). Lineweaver–Burk reciprocal plots of initial velocity and substrate concentrations (0.1–1 μM) are presented. Lines were derived from a weighted least-squares analysis of data.

To further characterize MAO inhibition by DPH6, reversibility study of this inhibitor was addressed. Irreversible inhibition was observed in both isoforms since enzyme activities were not significantly reverted after three consecutive centrifugations and washings with phosphate buffer (Fig. 2) followed by a pre-incubation with the inhibitor. Simultaneously, and for comparison purpose, the same assay was performed with irreversible MAO A inhibitor clorgyline and irreversible MAO B inhibitor l-deprenyl.

Next, the assessment of time-dependent inhibition of both MAO isoforms with **DPH6** was assessed by pre-incubating the enzyme with the inhibitor at times ranging 0–360 min (Fig. 3A). Samples with no compound were used to determine the maximum enzyme activity. Enzyme inactivation was not achieved before a pre-incubation of 180 min and 120 min for MAO A and MAO B, respectively, revealing time-dependent inhibition in both isoforms. These findings were confirmed by determining a constant variation on IC_{50} values as longer pre-incubations with **DPH6** were performed with both MAO isoforms (Fig. 3B, C and D).

2.2.3. Assessment of metal-chelating properties

Metal-chelating properties of compound **DPH6** were also investigated towards biometals Cu(II), Fe(III) and Zn(II) by UV–VIS spectrometry. The increase on brain levels of iron, zinc and particularly copper is reported to actively contribute to the formation of senile plaques by generating more reactive oxygen species through the A$\beta_{1\text{-}42}$-metal complex [21].

Upon the addition of varying concentrations of $CuSO_4$, $Fe_2(SO_4)_3$ or $ZnSO_4$, the maximum absorption detected at 240 nm with the compound alone shifted to 257 nm, exhibiting the formation of complexes **DPH6**-Cu(II), **DPH6**-Fe(III) and **DPH6**-Zn(II) (Fig. 4A–C). Significant variations on complexation times were observed depending on the metal. No spectral differences were identified when Cu(II) and was added after 5-min incubation whereas 1 h or O/N incubations were required to detect the formation of **DPH6**-Zn(II) and **DPH6**-Fe(III) complexes, respectively. These results confirm that **DPH6** selectively complexes Cu(II) salts. The equations obtained by the Job's method provided a solution at a mole fraction of 0.65 for compound **DPH6** complexing Cu(II) and Zn(II) and a mole fraction between 0.5 and 0.6 for the complex **DPH6**-Fe (III). This data revealed a 2:1 stoichiometry for all complexes.

2.3. Molecular modeling of DPH6

2.3.1. Inhibition of EeAChE

A modeling study was carried out through docking simulations for the purpose of gaining insights on the nature and spatial location of the key interactions of the (*R*)- and (*S*)-enantiomers of **DPH6** modulating the inhibitory activity of AChE and BuChE. As in our previous studies, we have chosen the 3D structure of the enzyme species (*Ee*AChE and eqBuChE) used for the kinetic studies. The kinetic data provide evidence that compound **6** displays a mixed

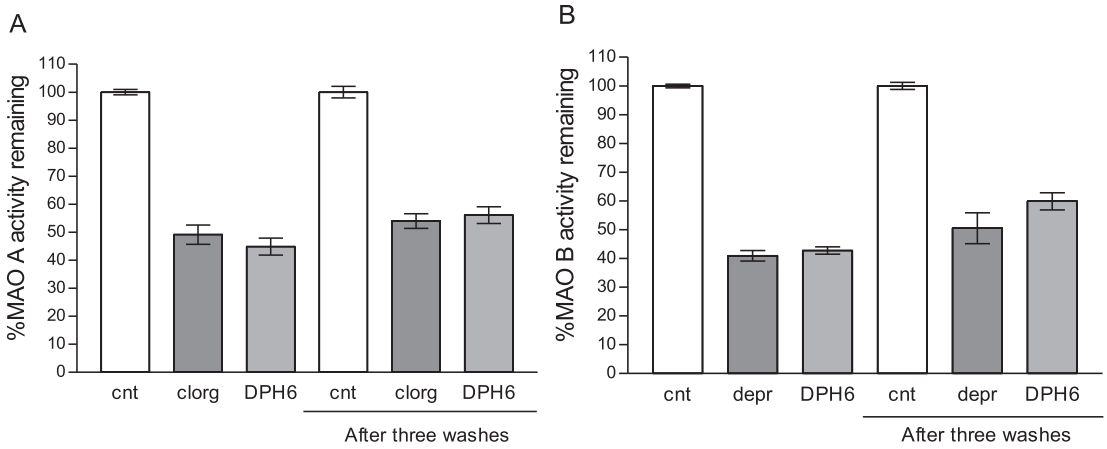

Fig. 2. (A) Reversibility study of MAO A inhibition by 10 μM **DPH6** and 50 nM clorgyline. (B) Reversibility study of MAO B inhibition by 20 μM **DPH6** and 20 nM l-deprenyl. MAO A and MAO B inhibition was performed following a 30-min pre-incubation. After three consecutive washes with buffer MAO activity was not significantly reverted. Data expressed as the mean ± SEM of six independent experiments in triplicate. Kruskal–Wallis one-way analysis was used.

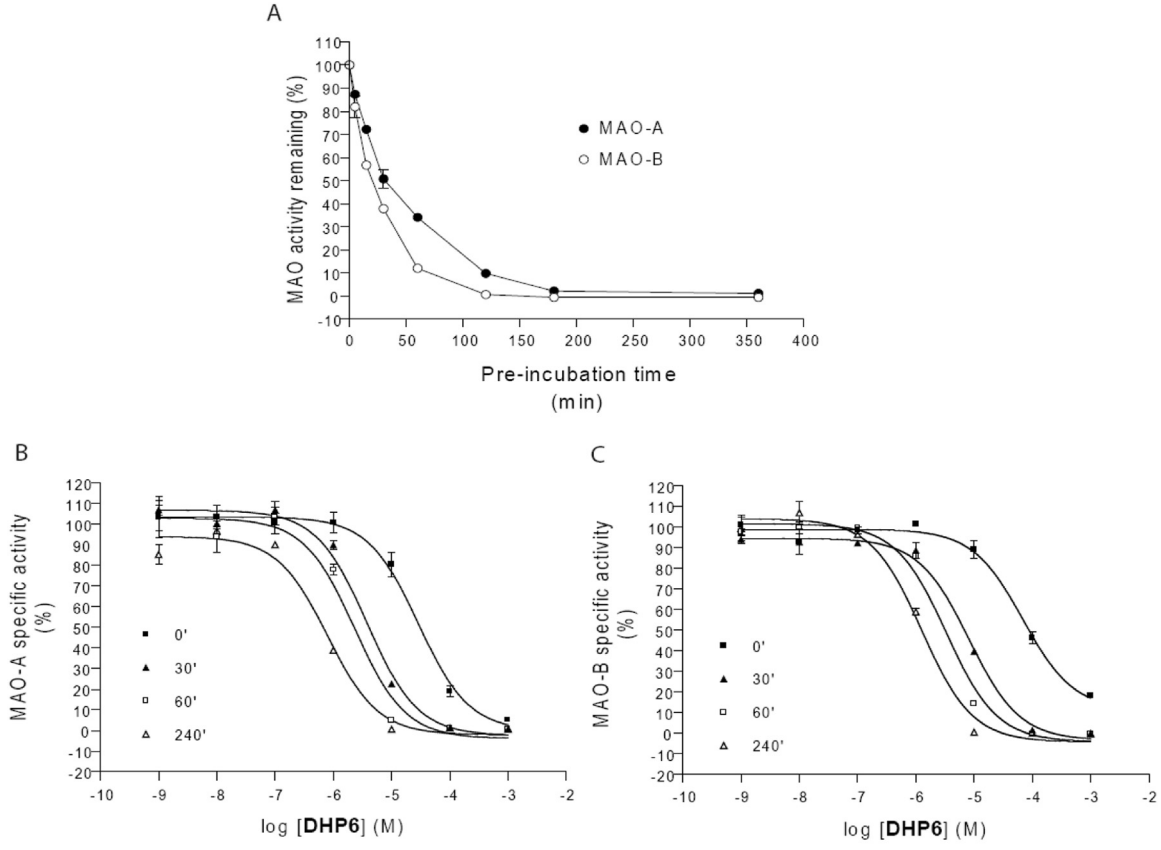

D

IC_{50} (μM) by pre-incubation time (min)

	0	30	60	240
MAO A	29.1	3.8	2.3	0.7
MAO B	61.7	8.3	3.3	1.2

Fig. 3. (A) Study of time-dependent inhibition of MAO A and MAO B by **DHP6** (10 μM and20 μM, respectively) over different pre-incubation times (0–360 min). (B and C) Dose-response curves (IC_{50}) following different pre-incubation times (0–240 min) with **DPH6** inhibiting MAO A and MAO B. (D) IC_{50} values determined following different pre-incubations. Data are the mean ± SEM of three independent experiments in triplicate.

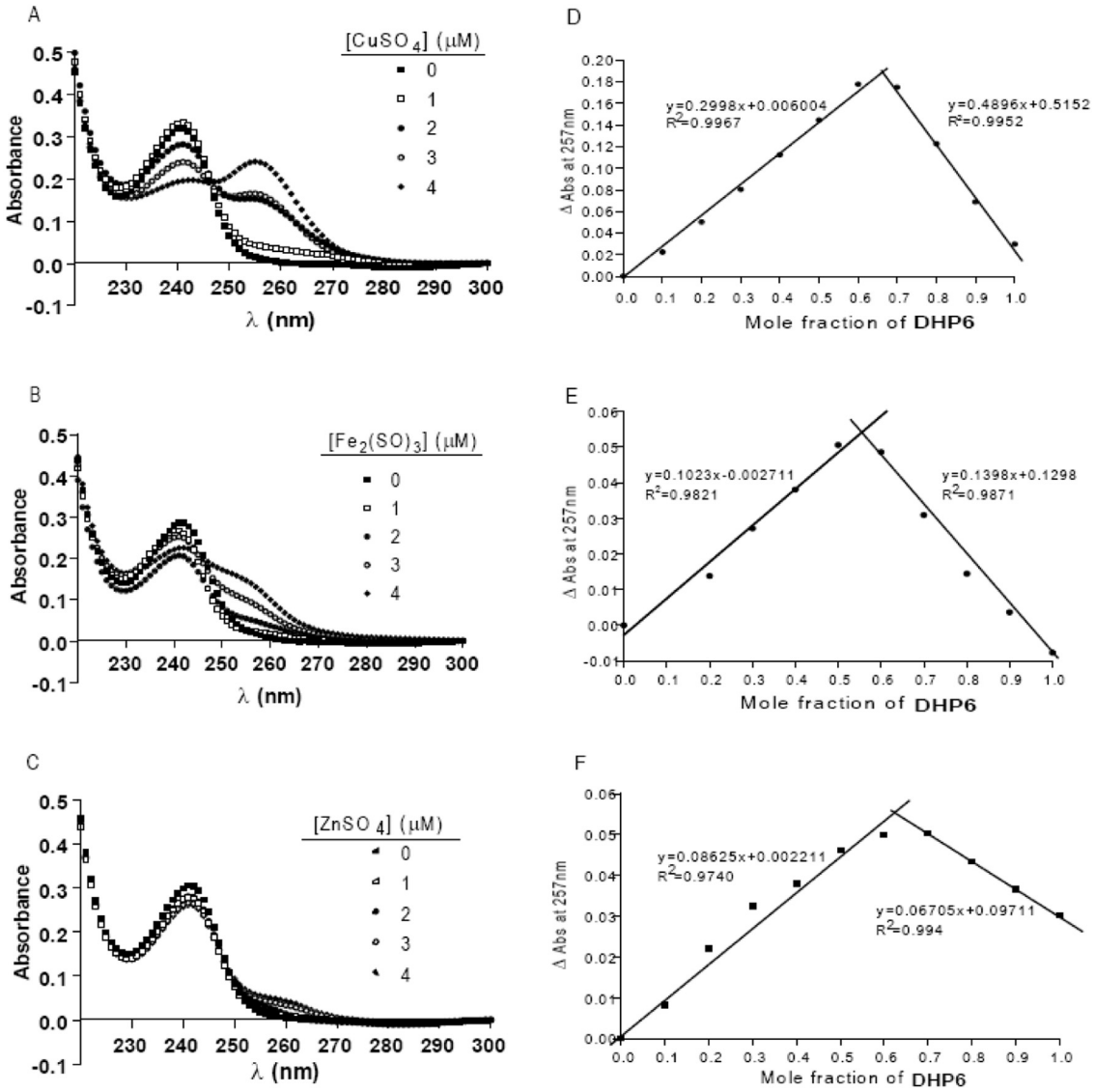

Fig. 4. (A) UV–VIS spectrum of a solution containing 10 μM **DPH6** and 0–4 μM $CuSO_4$ following 5-min incubation. (B) UV–VIS spectrum of a solution containing 10 μM **DPH6** and 0–4 μM $Fe_2(SO_4)_3$ following O/N incubation. (C) UV–VIS spectrum of a solution containing 10 μM **DPH6** and 0–4 μM $ZnSO_4$ following 1-h incubation. (D) Determination of the stoichiometry of complex **DPH6**-Cu(II), (E) complex **DPH6**-Fe(III) and (F) complex **DPH6**-Zn(II) following 5-min, O/N and 1-h incubation, respectively by using the Job's method. All solutions were prepared in distilled water and incubations performed at room temperature.

type inhibition and argue in favor of interactions of **DPH6** with both catalytic and peripheral binding sites of AChE. Molecular modeling studies have been carried in order to validate this assumption. Ligand docking studies were performed with Autodock Vina [22] using a single catalytic sub-unit of *Ee*AChE (PDB: 1C2B). This docking procedure allows the docking of ligands on the entire protein surface, without prior specification of the binding site. As in previous studies, the recognition process between (*R*)- and (*S*)-enantiomers of **DPH6** was theoretically investigated by flexible docking experiments. Flexible torsions in the ligands were assigned and protein side chain flexibility was incorporated allowing the rearrangement of the side chains of eight residues, Trp286, Tyr124, Tyr337, Tyr72, Asp74, Thr75, Trp86 and Tyr341. These residues delineate the shape of the gorge entry and lining and their motion may significantly enlarge the gorge to facilitate bulky ligand access to the catalytic site [23,24]. As shown in Figs. 5 and 6, it appears that both enantiomers of **DPH6** interact simultaneously with both catalytic and peripheral site of *Ee*AChE thanks to a linker of appropriate length showing a strong correlation with the observations we have from Lineweaver–Burk plots.

2.3.1.1. Docking studies of (R)-DPH6 with EeAChE. Computational docking studies of (*R*)-**DPH6** with *Ee*AChE yielded four major binding modes at the enzyme binding site. In Fig. 7, the four most favored binding modes are presented along with the first shell of residues surrounding (*R*)-**DPH6**.

Mode I and Mode II (Fig. 5A and B) placed the quinoline moiety near the opening of the binding pocket. Mode III and Mode IV (Fig. 5C and D) placed the quinoline deep into the binding pocket next to the residues known to be involved in catalysis. The classical catalytic triad is shaded in green in all four panels. A close examination of (*R*)-**DPH6** in Mode I revealed that the interaction with the AChE peripheral site involved a face to face π–π stacking between the indole ring of Trp286 and the quinoline moiety and a T-shaped π–π stacking between the phenyl ring of Tyr72 and the quinoline moiety. Besides, in this complex, a bifurcated hydrogen bond was

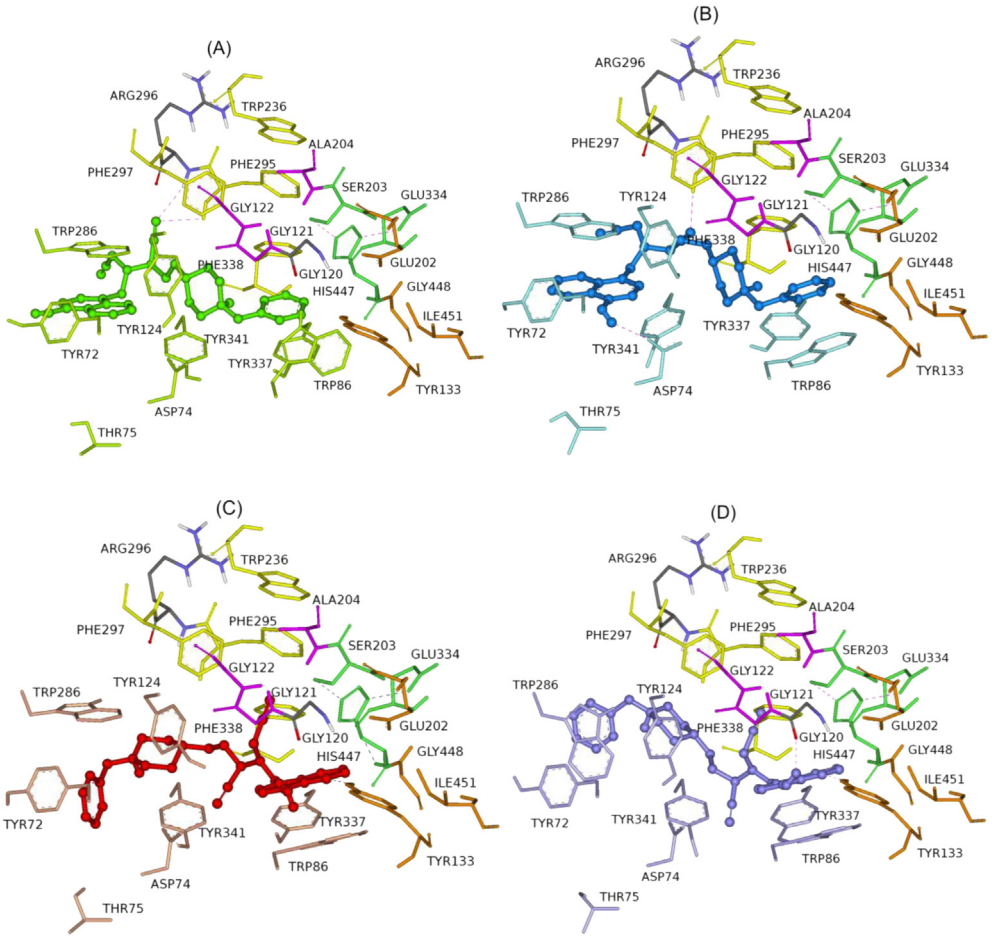

Fig. 5. Binding mode of inhibitor (*R*)-DPH6 at the active site of *Ee*AChE. (A) Mode I, compound (*R*)-**DPH6** is illustrated in green. (B) Mode II, compound (*R*)-DPH**6** is illustrated in blue. (C) Mode III, compound (*R*)-DPH**6** is illustrated in red (D) Mode IV, compound (*R*)-**DPH6** is illustrated in violet. Ligands are rendered as sticks and the side chains conformations of the mobile residues are illustrated in the same color light as the ligand. Different subsites of the active site were colored: catalytic triad (CT) in green, oxyanion hole (OH) in pink, anionic sub-site (AS) in orange, except Trp86, acyl binding pocket (ABP) in yellow, and peripheral anionic subsite (PAS) in blue. Black dashed lines are drawn among atoms involved in hydrogen bond interactions. (For interpretation of the references to colour in this figure legend, the reader is referred to the web version of this article.)

formed between the *nitrogen atom of the cyano group and Arg296-NH and Phe295-OH.* The benzyl moiety pointed towards the bottom of the gorge and established edge-to-face π–π interactions with Trp86 and face-to-face π–π interactions with Tyr337. In Mode II, the benzyl and the quinoline moieties interacted with Trp86 of the catalytic pocket and Trp286 of the peripheral site, respectively. In the middle of the gorge, *the nitrogen atom of the cyano group forms a hydrogen bond with the hydroxyl group of the Phe295*. At the

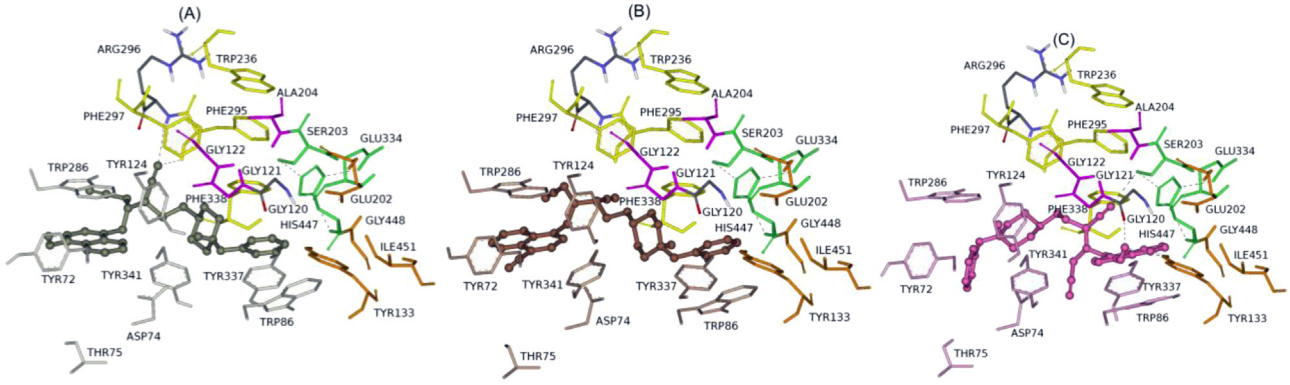

Fig. 6. Binding mode of inhibitor (*S*)-DPH6 at the active site of hAChE. (A) Mode I, compound (*S*)-**DPH6** is illustrated in gray. (B) Mode II, compound (*S*)-**DPH6** is illustrated in brown. (C) Mode III, compound (*S*)-**DPH6** is illustrated in pink. Ligands are rendered as sticks and the side chains conformations of the mobile residues are illustrated in the same light color as the ligand. Different subsites of the active site were colored: catalytic triad (CT) in green, oxyanion hole (OH) in pink, anionic sub-site (AS) in orange, except Trp86, acyl binding pocket (ABP) in yellow, and peripheral anionic subsite (PAS) in blue. Black dashed lines are drawn among atoms involved in hydrogen bond interactions. (For interpretation of the references to colour in this figure legend, the reader is referred to the web version of this article.)

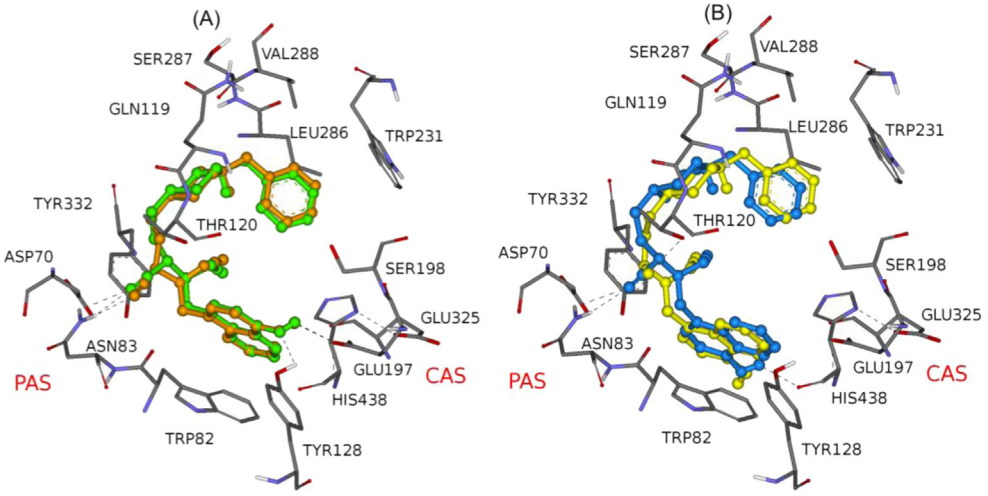

Fig. 7. Complex of compound (*R*)-DPH6 and (*S*)-DPH6 and eqBuChE homology built 3D-model. (A) Mode I, compound (*R*)-**DPH6** is illustrated in orange and compound (*S*)-**DPH6** in green. (B) Mode II, compound (*R*)-**DPH6** is illustrated in yellow and compound (*S*)-**DPH6** in blue. The compounds are rendered as sticks. (For interpretation of the references to colour in this figure legend, the reader is referred to the web version of this article.)

top of the gorge, the hydroxyl group of the quinoline moiety forms a hydrogen bond with the carboxylate group of Asp74. As can be seen in Fig. 5C (Mode III), (*R*)-**DPH6** has several interactions along the active-site gorge of *Ee*AChE. At the top of the gorge, the benzyl ring and Trp286 indole ring formed a favorable T-shaped π–π interaction. Near the bottom of the gorge the quinoline moiety stacked against the Trp86 indole ring. In this region, the nitrogen atom of the quinoline moiety was hydrogen bonded to the hydroxyl group of Tyr133. Comparison of Mode IV (Fig. 5D) and Mode III (Fig. 5C) revealed a broadly similar interaction but with two key differences: a) a significant movement of the Trp286 indole and benzyl rings in order to establish a face-to-face π–π interaction, and b) the rotation of the hydroxyl group of the quinoline moiety to form a hydrogen bond with the carbonyl group of Gly120. In both poses (Mode III and Mode IV), the three methylene units in the spacer of (*R*)-**DPH6** were long enough to allow a proper interaction between (*R*)-DPH**6** and both sites of the enzyme. The linker was lodged in a narrow cavity described by Asp74, Tyr124, Phe297, Tyr337, Phe338, and Tyr341. The protonated nitrogen was favorably interacting with the residues of a kind of "electrostatic cage" (Tyr124, Asp74, Tyr337 and Tyr341 side chains).

2.3.1.2. Docking studies of (S)-DPH6 with EeAChE. Docking studies of (*S*)-**DPH6** with *Ee*AChE yielded three major binding modes at the enzyme binding-site. In Fig. 6 the three most favored binding modes are presented along with the first shell of residues surrounding (*S*)-**DPH6**. Mode I and Mode II (Fig. 6A and B) placed the quinoline moiety near the opening of the binding pocket. Mode III (Fig. 6C) placed the quinoline deep into the binding pocket next to the residues involved in catalysis. In Mode I (Fig. 6A), the main stabilizing factors that keep stable the (*S*)-**DPH6**-AChE complex were found to be the hydrophobic contacts, π–π interactions and hydrogen bonding interactions. Compound (*S*)-**DPH6** can simultaneously bind at both the peripheral anionic site (PAS) and the catalytic active site (CAS) of *Ee*AChE. (*S*)-**DPH6** is able to bind in the PAS by face-to-face and edge-to-face π–π interactions between the quinoline moiety of the ligand and the Trp286 indole ring and the Tyr72 phenyl ring, respectively. Other interactions like a bifurcated hydrogen bond between the nitrogen atom of the cyano group and Arg296-NH and Phe295-OH could also play an important role in positioning and stabilizing the ligand inside the active site gorge. The benzene ring of (*S*)-**DPH6** formed a π–π stacking interaction with Trp86. In Mode II (Fig. 6B), compound (*S*)-**DPH6** can also adopt a similar binding conformation to that in Mode I. The ligand had an orientation along the active-site gorge, extending from the anionic sub-site of the active site at the bottom, to the peripheral anionic site at the top, *via* aromatic stacking interactions with Trp86, Trp286 and Tyr72 residues (Mode II, Fig. 6B). Conversely, in this orientation, compound (*S*)-**DPH6** was not able to form hydrogen bonds but a stronger stacking interaction between benzene ring and Trp86. Mode III (Fig. 6C) also placed the ligand along the active-site gorge. The quinoline ring formed a π–π interaction with the indole ring of Trp86 and also established three additional hydrogen bonds, which have an important contribution to the binding potency of the ligand. The hydroxyl group of Tyr133 formed two hydrogen bonds with the nitrogen and the hydroxyl group of the quinoline moiety, the later group is also hydrogen bonded to the carbonyl oxygen from the backbone of Gly120. On the other hand, at the peripheral anionic site (PAS), the benzene ring of the ligand form edge-to-face π–π interaction with the indole ring of Trp286 and with the benzene ring of Tyr72. In comparison with the other poses, the cyano residue is involved in the interactions with the catalytic triad of the active site gorge. This group is able to bind by mean of hydrogen bond with the Ser203 side chain.

On the basis of the similar orientation and the set of interactions, which were identified between the (*R*) enantiomer (Modes I-III, Fig. 5A–C) and (*S*) enantiomer (Modes I-III, Fig. 6A–C) and the protein residues within the gorge, it can be hypothesized that both enantiomers of **DPH6** could simultaneously bind at both the peripheral anionic site (PAS) and the catalytic active site (CAS) of *Ee*AChE.

2.3.2. Inhibition of eqBuChE

With respect to BuChE, in the absence of X-ray structure of eqBuChE, a homology model was used. The modeling of the 3D structure was performed by an automated homology-modeling program (SWISS-MODEL) [25–27]. A putative three-dimensional structure of eqBuChE has been created based on the crystal structure of human BuChE (pdb: 2PM8), as these two enzymes exhibited 89% sequence identity. In order to simulate the binding of both enantiomers of compound **DPH6** to eqBuChE, docking experiments were performed as blind dockings following the same

computational protocol used for *Ee*AChE. The best-ranked docking solutions revealed that BuChE can effectively accommodate both enantiomers of **DPH6** inside the active site gorge and two major binding modes can be proposed (Fig. 7). Modes I and II (Fig. 7A and B) for both enantiomers placed the quinoline moiety into the binding pocket next to the residues involved in catalysis. In this orientation, the phenyl moiety interacts with Trp231 by means of hydrophobic interactions and Trp82 allowed a π–π stacking interaction with the quinoline ring of the ligand. In Mode I (Fig. 7A), a close examination of the first shell of residues surrounding (*R*)-**DPH6** and (*S*)-**DPH6** revealed that in both enantiomers the hydroxyl group of the quinoline ring formed one hydrogen bond with the carboxylate group of Glu197 and another one with the hydroxyl group of the Tyr128. Moreover, the cyano group for the (*R*)-DPH**6** enantiomer, formed a hydrogen bond with the NH_2 of the side chain of Asn83, this bond was bifurcated in the case of (*S*)-**DPH6** enantiomer. In this orientation, hydrophobic interactions with the catalytic triad residues, Ser198 and His438 were found. In mode II (Fig. 7B), only one hydrogen bond was observable for the (*R*) enantiomer, it was formed between the cyano group and the hydroxyl group of Thr120. The (*S*) enantiomer preserved the cyanide bifurcated hydrogen bond already observed in Mode I, and the hydroxyl group of the quinoline ring established a hydrogen bond with the catalytic triad residue His438.

Analysis of the intermolecular interactions indicated key residues responsible for ligand binding. The cyanide group is likely to be an important feature for these derivatives to exhibit BuChE inhibitory activity.

2.3.3. Inhibition of MAO A and MAO B

In order to explore the nature of the ligand–receptor interactions, the ligand was docked to the active site of both MAO A and MAO B isoforms using the program Autodock Vina [22]. We have focused on DPH**6**, which showed the best both MAO A ($IC_{50} = 1.8 \pm 0.1$ μM) and MAO B ($IC_{50} = 1.6 \pm 0.25$ μM) inhibitory activities, with significant *Ee*AChE and eqBuChE inhibitory potencies. Although rat MAO A (rMAO A) and rat MAO B (rMAO B) are ~90% identical in sequence with human enzymes, their functional properties are similar but not identical to those of human enzymes. Given that MAO inhibition assays were carried out on rat brain mitochondria, docking experiments were carried out using the X-ray structure of rMAO A (PDB ID: 1O5W) and the homology model of rMAO B developed from a human MAO B (hMAO B) crystallographic structure (PDB ID: 1S3E) [28], as previously described for eqBuChE. The recognition process between (*R*)- and (*S*)-enantiomers of **DPH6** (chosen as reference compound) was theoretically investigated by blind docking experiments, in accordance with a protocol previously defined by us and well validated [29]. The enzyme–inhibitor interactions might allow a theoretical evaluation of which enantiomer of the inhibitor could be better accommodated into the catalytic site of MAO A and MAO B. Results from several studies have shown that it must be the neutral amine that reaches the active site of MAO A and MAO B to allow the chemistry [30–33]. Therefore, the docking simulations were done using both enantiomers of **DPH6** as neutral species despite of at physiological pH, most of the piperidine rings would be in the protonated, positively charged form. In docking with MAO A, during each run, the side chains of twenty-one residues (Tyr 69, Leu97, Gln99, Ala111, Phe112, Tyr124, Trp128, Phe173, Leu176, Phe177, Ile180, Asn181, Ile207, Phe208, Gln215, Cys323, Ileu325, Ileu335, Phe352, Tyr407 and Tyr444) were allowed to relax with the ligand, while the remainder of the enzyme was fixed in 3-D space. Six water molecules labeled as w72, w193, w11, w23, w15, and w53 in accordance with the numbering reported for the hMAO B crystallographic structure (PDB ID: 1S3E) located near the FAD cofactor were considered as integral components of the protein structure during the docking simulation. Docking of **DPH6** was performed for both enantiomers and a sole binding mode per enantiomer was found. Fig. 8A and B illustrated the binding modes of (*R*)-**DPH6** and (*S*)-**DPH6** enantiomers into the hMAO A binding cavity. Both enantiomers showed a relatively similar localization for the hydroxy-quinoline and benzyl moieties, with the rest of the molecule easily accommodated in the relatively large cavity of MAO A.

2.3.3.1. Inhibition of MAO A by (R)- and (S)-DPH6. Fig. 8A showed that the optimal position for the (*R*)-**DPH6** enantiomer placed the quinoline ring in an "aromatic cage" formed by Tyr407, Tyr444 side chains, as well as the isoalloxazine FAD ring. (*R*)-**DPH6** forms π–π stacking interactions with Tyr407 and the carbonyl group of Gln215 residue. The hydroxy-quinoline moiety was involved in two hydrogen bonds between the OH and the carbonyl oxygen of the FAD and the 193w molecule. The benzyl group is located in a hydrophobic core delimited by residues Phe173, Phe208, Ileu325, Ala111 Phe112 and Leu176. The cyano group is also able to form a hydrogen bond with Cys323 side chain. Compound (*S*)-**DPH6** showed a binding geometry very similar to that displayed by (*R*)-**DPH6** as for the hydroxy-quinoline and benzyl moieties (see Fig. 8B), which displayed a set of intermolecular interactions described before in the case of the (*R*)-enantiomer. The main difference with respect to the recognition of (*R*)-**DPH6** was in the spatial orientation of the propargyl, piperidine and cyano groups, the later accommodated this time to establish hydrogen bond with Thr336 residue. The docking studies rationalized the relevant inhibitory activity of **DPH6** towards MAO A, as due to the formation of several favorable interactions with the catalytic site of the enzyme.

The importance of the cyano group in properly positioning the ligand by H-bond formation is pointed out. It is worth noting that compounds lacking this CN, like in the case of **DPH7**, showed the inhibitory activity drastically lowered.

2.3.3.2. Inhibition of MAO B by (R)- and (S)-DPH6. To rationalize the selectivity towards MAO A and MAO B of (*R*)- and (*S*)-**DPH6**, blind docking studies of **DPH6** into the MAO B were done. Up to date, a reliable 3-D structure of rMAO B is not available and we used a 3D homology model of rMAO B for the docking studies. The six structural water molecules selected for rMAO A were also included in the model. For MAO B, the inhibitor (*R*)-**DPH6** crosses both cavities, presenting the piperidine nucleus located between the "entrance" and "catalytic" cavities, separated by the residues Ile199 and Tyr326. This complex was stabilized by hydrophobic contacts of quinoline ring with Phe103, Pro104, Trp119, His90, Val316 and Tyr115. Besides, the phenyl ring is hosted into the "aromatic cage" framed by Tyr398, Phe343, Tyr435, and the FAD aromatic ring, where it forms a number of π–π interactions also including Gln206. No intermolecular H-bonds between ligand and enzyme were observed (Fig. 9A). For MAO B, the quinoline system of the inhibitor (*S*)-DPH**6** was hosted in the entrance cavity made up by lipophilic residues Phe103, Pro104, Trp119, His90, Ileu164, Val316 and Tyr115. The phenyl ring occupied the substrate cavity and was in direct contact with the Tyr398, Phe343, Tyr435, and the FAD aromatic ring. The compound established a H-bond with Tyr115 OH hydrogen by its OH oxygen (Fig. 9B). The study confirmed the selectivity of **DPH6** for MAO A isoform. Selectivity is likely due to the orientation of the quinoline and phenyl moieties of **DPH6** in MAO A and in MAO B. For MAO B, the quinoline system was hosted in the entrance cavity and for MAO A this system occupied the substrate cavity. In this disposition the quinoline moiety interacted directly with the FAD aromatic ring.

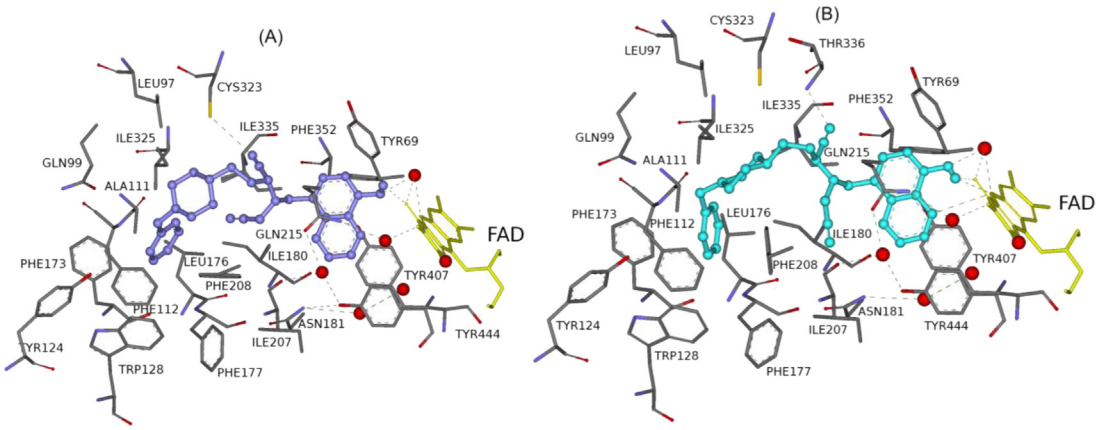

Fig. 8. Docking poses of inhibitor **DPH6** into rMAO A. (A) (*R*)-**DPH6** (purple sticks). (B) (*S*)-**DPH6** (blue sticks). Amino acid residues of the binding site are color-coded. The flavin adenine dinucleotide cofactor (FAD) and the six water molecules are represented as an integral part of the MAO A structure model and are rendered as yellow sticks and red balls, respectively. Green dashed lines are drawn among atoms involved in hydrogen bond interactions. (For interpretation of the references to colour in this figure legend, the reader is referred to the web version of this article.)

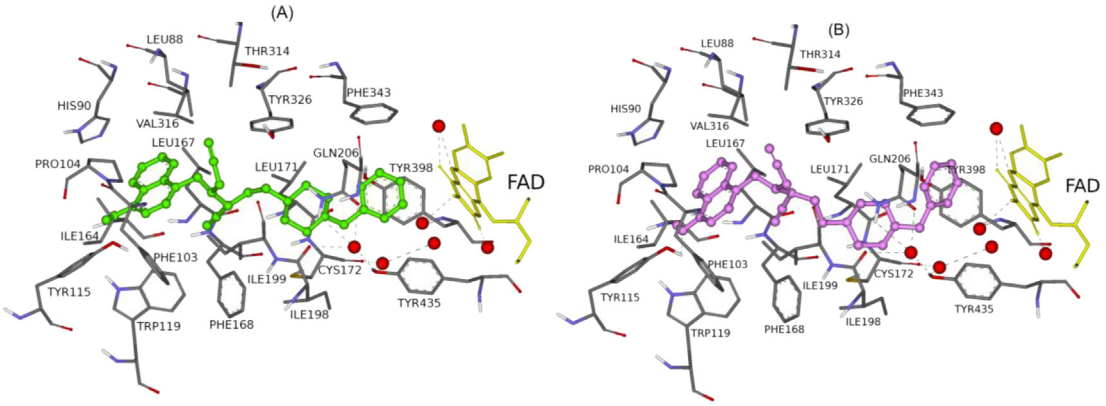

Fig. 9. Docking pose of inhibitor **DPH6** into rMAO B. (A) (*R*)-**DPH6** (green sticks). (B) (*S*)-**DPH6** (pink sticks). Amino acid residues of the binding site are color-coded. The flavin adenine dinucleotide cofactor (FAD) and the six water molecules are represented as an integral part of the MAO B structure model and are rendered as yellow sticks and red balls, respectively. (For interpretation of the references to colour in this figure legend, the reader is referred to the web version of this article.)

2.3.4. *Predicted binding affinities*

AutoDock Vina provides a computed binding affinity for each docking mode predicted. Binding affinity data for both enantiomers with the four enzymes are summarized in Table 2. The more negative the value, the tighter the predicted bonding. For the (*R*)-**DPH6** interaction with the AChE, predicted binding affinities were very similar for the four modes (I–IV), ranging from −11.0 to −12.3 kcal/mol. Predicted binding affinities for (*R*)-**DPH6** with BuChE (−10.4 and −10.7 kcal/mol) were slightly lower in range than those for the AChE complex (Table 2). Data for (*S*)-**DPH6** interactions gave very similar predicted binding than that for (*R*)-**DPH6** interactions: predicted binding energies of −11.5 to −12.4 kcal/mol for AChE and −9.9 and −9.7 kcal/mol for BuChE. Consistent with biological trends, both enantiomers were predicted to have similar binding interactions with AChE and BuChE. The weakest predicted binding affinities were computed for the both enantiomers interactions with the MAO A and MAO B enzymes. Very similar binding affinity values were also observed for both enantiomers with MAO A and MAO B.

Table 2
Predicted binding affinities (kcal/mol).

DPH	Mode	*Ee*AChE	EqBuChE	MAO A	MAO B
(*R*)-**DPH6**	I	−11.0	−10.4	−7.8	−8.9
	II	−12.3	−10.7		
	III	−12.1			
	IV	−12.1			
(*S*)-**DPH6**	I	−11.9	−9.9	−7.9	−8.8
	II	−11.5	−9.7		
	III	−12.4			

2.4. *Theoretic ADMET analysis of DPH hybrids*

ADMET properties are important conditions and major parts of pharmacokinetics. Viable drugs should have proper ADMET properties to be approved as a drug in clinical tests. The drugs used for neurological disorder treatment, such as AD, are generally CNS acting drugs, so factors that are important to the success of CNS drugs were analyzed. In particular, the new molecules should present a good CNS penetration profile and low toxic effects. Current *in silico* ADMET predictions cannot fully replace well-established in vitro cell-based approaches or *in vivo* assays, but they can provide significant insights [34]. Computer predictions were performed with ADMET Predictor 6.53 [35] and ACD/Percepta 14.0.04 [36] software packages. According to the predictions (Table 3), the lipophilicity increases with the hydrocarbon tether

Table 3
Calculated physicochemical properties for DPH1-7.[a,b]

	Molecular weight	No. of H-bond donors	No. of H-bond acceptor	No. of rotatable Bonds[a]	logP (Moriguchi)[a,c]	logP[a]	TPSA	No. violations Lipinski's rule	LogBB[a,d]
1	385.51	1	4	6	3.55	3.79	39.60	0	−0.12
2	424.55	1	5	6	3.09	3.51	63.39	0	−0.31
3	399.54	1	4	7	3.75	4.16	39.60	0	0.03
4	438.58	1	5	7	3.29	3.76	63.39	0	−0.14
5	413.57	1	4	8	3.95	4.54	39.60	0	0.20
6	452.60	1	5	8	3.48	4.05	63.39	0	0.07
7	427.59	1	4	9	4.09	4.95	39.60	0	0.36
Donezepil	379.50	0	4	6	3.52	4.59	38.78	0	0.88
M-30	226.28	1	3	3	2.06	2.32	36.36	0	0.17

	LogBB[b,d]	logPS[e]	Log (PS*fu, brain)[e]	Peff (cm/s × 10^4)	Human intestinal absorption (%)[f]	In vitro Caco-2 perm (nm/sec)[g]	MDCK (cm/s × 10^7)[h]	% Plasma protein binding (in vitro)[i]	Toxicity[a]
1	−0.02	−1.6	−2.8	4.47	96.79	45.66	350.7	72.68	hERG
2	−0.11	−1.6	−2.9	3.36	96.83	49.28	348.2	80.31	hERG
3	0.29	−1.5	−3.0	4.99	96.84	52.26	325.9	76.37	hERG
4	0.26	−1.6	−3.1	3.75	96.91	51.96	321.9	78.44	hERG
5	0.36	−1.4	−3.2	5.59	96.87	54.36	313.0	77.11	hERG
6	0.34	−1.5	−3.3	4.18	96.99	54.37	306.1	79.97	hERG
7	0.46	−1.4	−3.4	6.24	96.90	54.08	301.9	77.40	hERG
Donezepil	0.31	−1.4	−3.0	6.69	97.95	55.51	306.4	84.62	hERG
M-30	−0.27	−1.5	−2.1	2.5	95.86	42.90	429.3	69.02	

[a] ADME Predictor, v.6.5.
[b] ACD/Percepta 14.0.
[c] Moriguchi model (ref. [4]).
[d] According to the classification made by Ma et al. [9]: High absorption to CNS: logBB more than 0.3; Middle absorption to CNS: logBB 0.3 ~ −1.0; Low absorption to CNS: logBB less than −1.0.
[e] Other estimated parameters related to brain penetration were used to classify the compounds as CNS permeable or non-permeable: rate of brain penetration (LogPS) is the rate of passive diffusion/permeability; brain/plasma equilibration rate (Log(PS*fu,brain)); fu,brain − fraction unbound in plasma.
[f] Human intestinal absorption is the sum of bioavailability and absorption evaluated from ratio of excretion or cumulative excretion in urine, bile, and feces. A value between 0 and 20% indicates poor absorption, 20−70% shows moderate absorption, and 70−100% indicates good absorption.
[g] Caco-2 cells are derived from human colon adenocarcinoma and possess multiple drug transport pathways through the intestinal epithelium. A value <4 indicates low permeability, 4−70 shows middle permeability, and >70 indicates high permeability.
[h] The MDCK cell system may be used as a good tool for rapid permeability screening. A value <25 indicates low permeability, 25−500 shows middle permeability, and >500 indicates high permeability.
[i] The percent of drug binds to plasma protein. A value <90% indicates weak binding, and >90% indicates strong binding to plasma proteins.

chain, and for the same value of *n*, the α-aminonitriles show the expected slightly lower lipophilicity. All of the **DPH** show good values (log $P < 5$ and mlog $P < 4.15$) [37], and as can be deduced, the whole series of structures meets the Lipinski's rule of five [38]. Moreover, a more severe rule for CNS drugs-like characteristics [39] (MW ≤ 450, HB donor ≤ 3, HB acceptors ≤ 7, log $P \leq 5$, PSA ≤ 90, and number of rotatable bonds ≤ 8) is satisfied for all structures, although the molecular weight of **DPH6** is on the borderline. However, drugs that penetrate CNS should have lower polar surface areas (PSA) than other kinds of molecules, being the optimal range 60−70 $Å^2$ [40]. Therefore, only the α-aminonitriles DPH fall in the suitable range of values.

The blood−brain barrier (BBB) is a separation of circulating blood and cerebrospinal fluid in the central nervous system (CNS), so an estimation of BBB penetration means predicting whether compounds pass across the blood−brain barrier. This is a crucial pharmacokinetic property in drug design because CNS-active compounds, such as those for AD, must pass across it. According to the computed values [41], for the same *n*, the α-aminonitriles present slightly lower values, whereas the values increase with the chain length. In any case, the two models predict that all structures should be moderate to good candidates, showing middle to high absorption to CNS. In particular, the **DPH3** and **DPHs 5**−**7** show the best results suggesting a brain penetration sufficient for CNS activity [42,43].

Generally, the degree to which any drug binds to plasma protein influences not only the drug action but also its disposition and efficacy. Usually, the drug that is unbound to plasma proteins will be available for diffusion or transport across cell membranes and thereby finally interact with the target. Herein, the percent of drug bound with plasma proteins was estimated and the compounds were predicted to be weakly bind to plasma proteins.

Other ADMET predictions of the present **DPH** compounds show satisfactory results. Thus, all of them show good intestinal absorption (HIA [44] of about 96% and effective permeability across the intestinal membrane [45], Peff > 0.1), moderate apparent permeability for in vitro MDCK cells (>25) [46] and middle permeability for in vitro Caco-2 cells [47]. Regarding toxicity properties, these compounds are predicted to show cardiac toxicity (hERG potassium channel blockage), but, according to the models used, they could lack carcinogenicity and hepatotoxicity [48−50].

In summary, these structures show moderate to good ADMET properties; in particular those with increasing values of *n* in the linker present proper drug-like properties and brain penetration capacity for CNS activity.

2.5. Toxicological evaluation of DPH6

Based on the predicted non hepatotoxicity (see above) of the **DHP** compounds, next we analyzed our hit **DHP6** hybrid in an in vitro toxicity test in HepG2 cells, determining the cell viability with MTT method [51], using donepezil as a reference molecule. The results shown in Table 4 are very interesting as they prove that **DPH6** is by far less toxic than donepezil at high concentrations (from 30 μM to 1000 μM), while at low concentrations (from 1 μM

Table 4
In vitro toxicity in HepG2 cells.[a]

Compounds	Viability (%) HepG2 cells						
	1 μM	3 μM	10 μM	30 μM	100 μM	300 μM	1000 μM
DPH6	98.4 ± 1.64^{ns}	94.8 ± 2.42 ^{ns}	94.4 ± 1.91^{ns}	92.4 ± 2.20 ^{ns}	85.6 ± 4.10*	71.44 ± 3.33***	51.5 ± 3.39***
Donepezil	98.6 ± 0.62^{ns}	97.0 ± 1.77 ^{ns}	92.4 ± 1.05*	83.5 ± 2.15***	80.0 ± 2.36***	53.4 ± 1.44***	40.9 ± 1.50***

$^{***}P \leq 0.001$, $^{**}P \leq 0.01$, $^{*}P \leq 0.05$ and ^{ns} not significant, with respect to control group. Comparisons between drugs and control group were performed by one-way ANOVA followed by the Newman–Keuls post-hoc test.

[a] Cell viability was measured as MTT reduction and data were normalized as % control. Data are expressed as the means ± s.e.m. of triplicate of four different cultures. All compounds were assayed at increasing concentrations (1–1000 μM).

to 10 μM) both are non toxic showing a very similar cell viability profile.

To sum up, hybrid **DPH6** preserves all the anti-cholinesterasic properties related to donepezil, but, as expected, shows an additional multipotent inhibitory activity in agreement with the in vitro results previously determined such as MAO inhibition capacity, biometal (Cu, Zn and Fe) chelating properties, favorable ADMET data and a notorious lack of hepatotoxicity. Consequently, and based on these in vitro pharmacological analyses, next we stepped forward to preliminary *in vivo* tests in order to investigate the potential biological profile of selected derivative **DPH6**.

2.6. Relief of scopolamine-induced long-term memory deficit in mice by DHP6

To analyze the *in vivo* effect on contextual memory, **DPH6** was administered to scopolamine-treated mice that were subjected to passive avoidance behavioral test. This task is based on contextual memory in which the hippocampus plays an important role, with the association between an environmental context that the animal learns to avoid and an aversive stimulus (foot-shock). This behavioral test has been extensively used to evaluate learning and memory in rodent models of central nervous system disorders and for screening of novel chemical entities on memory function [53,54]. Scopolamine, a well-known non-selective muscarinic antagonist that produces amnesic effects in both rodents and human, is frequently used to perform pharmacological assays for studying the effects of enhancers on cognitive functions [52]. During the training day, no significant differences in the latency time between treated groups were found (Fig. 10), even though scopolamine has been reported to influence motivational behavior [55]. In the probe session (Fig. 11), scopolamine (1 mg/kg)-induced cognitive deficits was reflected by a decreased latency in comparison to saline (vehicle) group ($^{***}p < 0.001$). Not surprisingly, donepezil + scop group showed a latency time similar to that observed in the vehicle group. Likewise, scopolamine effect was widely reversed in the **DPH6** + scop group ($^{***}p < 0.001$). Characteristically, not statistical difference in the latency time between **DPH6** + scop and donepezil + scop groups were observed and it was similar to that exhibited by the vehicle.

When comparing individual groups between training and probe sessions (Fig. 12), it is noteworthy that in the vehicle + scop group no significant differences were observed in the latency time. In striking contrast, during the probe session, handling groups: saline, donepezil + scop (1 mg/kg) and DPH6 + scop (35 mg/kg) remained in the brightly lit compartment for longer time than that measured in the training session, significantly increasing the latency time. The retention impairment observed in the probe session after a single dose of scopolamine (1 mg/kg), administered 30 min before training, is in good agreement with previous reports [56]. Taken these results together, we might conclude that both **DPH6** (35 mg/kg) and donepezil (1 mg/kgg) are able to induce similar effects on cognition.

3. Conclusion

DPHs 1–7, designed as hybrids from donepezil and M30, bearing N-benzylpiperidine and a pro-chelator 8-hydroxyquinoline moieties attached to a central N-propargylamine core, have been synthesized and subjected to pharmacological evaluation. DPHs 1–7 were readily prepared in good yields, in short synthetic sequences, from easily available precursors.

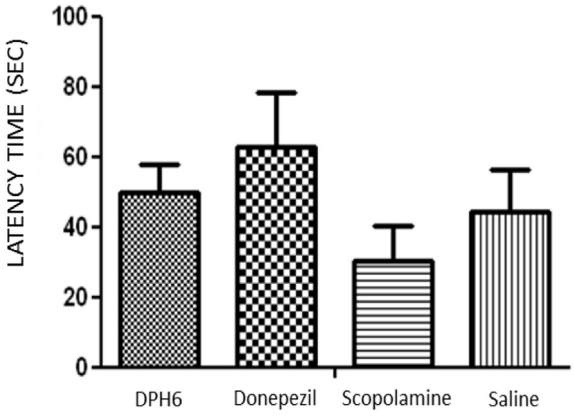

Fig. 10. Comparative effect of **DPH6**, donepezil and scopolamine on latency time in the training day. Bars represent the mean of latency time in seconds (sec) corresponding to each of experimental handling group No significant differences were found between groups. Values expressed as mean ± SEM of 8–10 independent experiments.

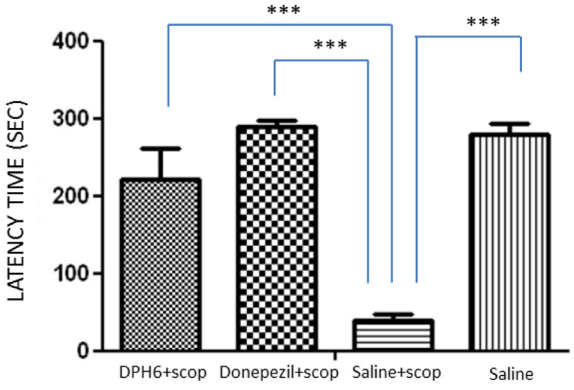

Fig. 11. Comparative effects on latency time of **DPH6** and donepezil on scopolamine-induced amnesia in the probe session. Bars represent the mean of latency time in seconds (sec) corresponding to each of experimental handling group. SEM is represented by error bars. Analysis of variance (ANOVA) followed by Bonferroni's post hoc test shows significant differences ($^{***}p < 0.001$) between groups **DPH6**, donepezil or vehicle with the scopolamine group. Values expressed as mean ± SEM of 8–10 independent experiments.

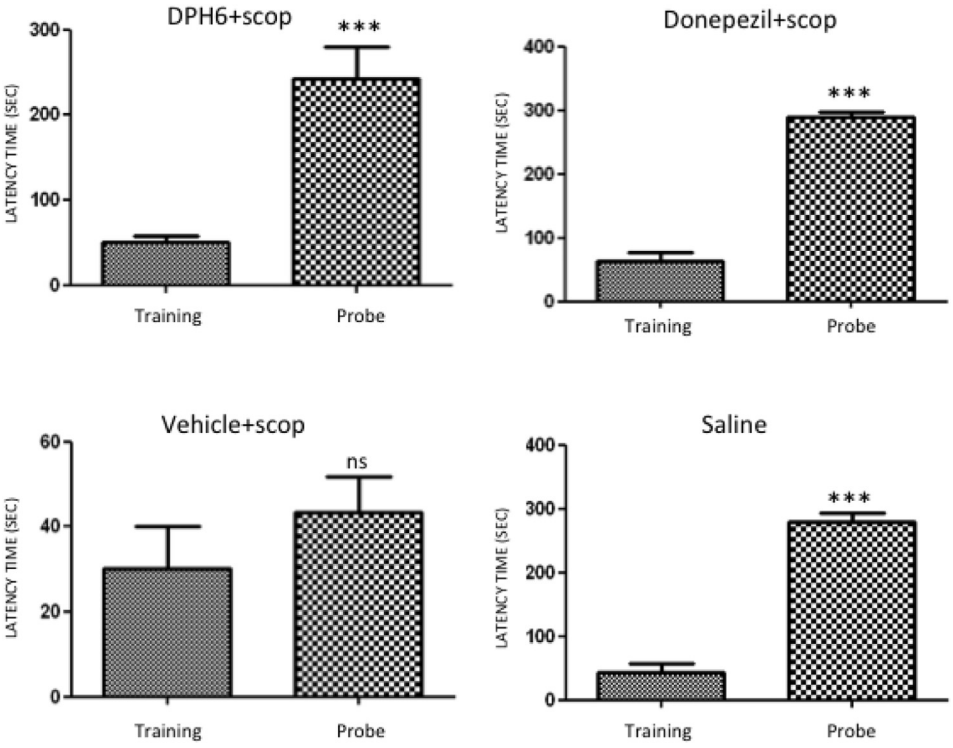

Fig. 12. Statistical differences within groups (training versus probe) determined by the Student's *t*-test (**$p < 0.01$; ***$p < 0.001$).

The biochemical evaluation of these molecules showed DPHs 2–7 hybrids as non-selective ChE and MAO inhibitors with moderate-to-low micromolar activity. Particularly interesting resulted DPH6, an irreversible MAO A/B, mixed-type EeAChE inhibitor able to complex biometals Cu(II) and Zn(II) and Fe(III). Compared to related M30A [15] (Chart 1), the demethylated derivative of M30 [15], or M30B [39] (Chart 1), DPH6 showed a very similar MAO inhibitory profile with biometal chelating properties.

Computational docking studies of (R)- and (S)-enantiomers of **DPH6** in AChE and BuChE yielded several binding modes for each enantiomer, but we have not observed significant differences between the binding energies of the different binding patterns for each enantiomer. For both MAO A and MAO B, only one binding mode has been proposed based on the most stable complex formed between the (R)- and (S)-enantiomers of **DPH6** and the enzymes, showing also very similar binding energies. In addition, we have discovered an essential role for the cyano group in properly positioning the ligand by hydrogen-bond formation with the amino acid residues of the binding sites of AChE, BuChE and MAO A. It is worth noting that compounds lacking the cyano motif, like in the case of **DPH7**, showed drastically lowered inhibitory activity. Finally, it is worth pointing out that α-aminonitriles have been seldom investigated as ChE inhibitors [40], and to the best of our knowledge, they have never been analyzed as MAO inhibitors [41]. However, some works have described nitriles as MAOIs [42], and Tipton and collaborators have reported that cyanide potentiates the inhibition of MAO by the irreversible inhibitor, phenelzine and pheniprazine [43]. One of the reviewers has kindly addressed our attention to the fact that "historically, prescribing MAO inhibitors have been reserved as a last–line of treatment because of potentially lethal effects due to drug interactions with a wide variety of therapeutic agents". Also, donepezil produces a wide assortment of side effects that include bradycardia, nausea, diarrhea, loss of appetite and stomach pain [44].

In addition, and according to the theoretic ADMET analysis, **DPH** compounds showed proper drug-like properties and brain penetration capacity for CNS activity. In particular, **DPH6** is lees toxic tan donepezil at high concentrations in an in vitro model of toxicity in HepG2 cells.

Finally, in terms of translational science, it is remarkable the *in vivo* effect of **DPH6** as enhancer on cognitive functions. Scopolamine induced memory deficits is greatly dependent on the cholinergic system [57]. We have found that donepezil is much more powerful than **DPH6** as cholinesterase inhibitor. This result is consistent with our own results on **ASS234** [8,9] (more potent ChEI than **DPH6**) which significantly lowers scopolamine-induced learning deficits in healthy adult mice, suggesting that product **ASS234** works as cognitive enhancer, as efficiently as donepezil at lower dosage, likely useful for the treatment of AD. Given the latter, the well-balanced anti-cholinesterasic and MAO inhibition profile in addition to the other attractive pharmacological properties of **DPH6** described here, and that **DPH6** has effect as enhancer on cognitive functions, prompt us to propose DPH6 as the first racemic α-aminonitrile identified so far as a multifunctional chelator for biometals, able to interact in two key enzymatic systems implicated in AD, and a new lead compound that deserves further investigation for the potential treatment of this disease.

To sum up, the well-balanced anti-cholinesterasic and MAO inhibition profile, in addition to the other attractive pharmacological properties described here, prompt us to propose **DPH6** as the first racemic α-aminonitrile that has been identified as a multifunctional chelator for biometals, able to interact in two key enzymatic systems implicated in AD, and a new lead compound that deserves further investigation for the potential treatment of this disease.

4. Experimental section

4.1. Chemistry

4.1.1. General methods

Melting points were determined on a Koffler apparatus, and are uncorrected. ^{1}H NMR and ^{13}C NMR spectra were recorded in $CDCl_3$ or DMSO-d_6 at 300, 400 or 500 MHz and at 75, 100 or 125 MHz, respectively, using solvent peaks [$CDCl_3$: 7.27 (*D*), 77.2 (*C*) ppm; and DMSO-d_6: 2.49 (*D*), 40 (*C*) ppm] as internal reference. The assignment of chemical shifts WAs based on standard NMR experiments (^{1}H, ^{13}C, DEPT, COSY, gHSQC, gHMBC). Mass spectra were recorded on a GC/MS spectrometer with an API-ES ionization source. Elemental analyses were performed at CNQO (CSIC, Spain). TLC were performed on silica F254 and detection by UV light at 254 nm or by charring with either ninhydrin, anisaldehyde or phosphomolybdic-H_2SO_4 dyeing reagents. Anhydrous solvents were used in all experiments. Column chromatography was performed on silica gel 60 (230 mesh). All known compounds have been synthesized as reported. All compounds were ≥95% purity as determined by examination of their combustion analyses.

4.1.2. 5-(Chloromethyl) quinolin-8-ol (**8**) [17]

To a cooled solution of 8-hydroxyquinoline (14.6 g, 100 mmol) in conc. HCl (44 mL) at 0 °C, a 37% aqueous formaldehyde solution (20 mL) was added. Then HCl (g) was bubbled through the solution with stirring for 2 h. The mixture was allowed to warm to rt with further stirring for 6 h and without stirring for 2 h more. The product was filtered and the solid was rinsed with conc. HCl, giving product **8** [17] (19.9 g, 77.5%).

4.1.3. 5-(((1-Benzylpiperidin-4-yl)(prop-2-ynyl)amino)methyl) quinolin-8-ol (DPH1)

To a solution of commercial 1-benzyl-4-piperidone (1.3 g, 7.0 mmol) and propargylamine (580 mg, 10.5 mmol) in MeOH (22 mL) at 0 °C, was added a small amount of CF_3CO_2H (5 drops). After being stirred for 1 h, $NaBH_3CN$ (1.3 g, 19.7 mmol) was added to the solution. The mixture was stirred at 0 °C overnight and then quenched with aqueous saturated $NaHCO_3$. The mixture was concentrated *in vacuo* and extracted with AcOEt. The combined organic layers were dried over $MgSO_4$ and concentrated under reduced pressure. The crude product was purified by column chromatography (SiO_2, AcOEt/MeOH = 4:1 v/v) to give 1-benzyl-*N*-(prop-2-ynyl)aminopiperidine (**9**) (500 mg, 31.2%) as an orange oil [R_f = 0.19 (AcOEt/MeOH = 4:1); ^{1}H NMR (400 MHz, $CDCl_3$) δ 1.34–1.49 (m, 2H), 1.76–1.88 (m, 2H), 2.00–2.15 (m, 3H), 2.17–2.22 (t, J = 2.3 Hz, 1H), 2.65–2.76 (m, 1H), 2.81–2.90 (m, 2H), 3.41–3.46 (d, J = 2.3 Hz, 2H), 3.52 (s, 2H), 7.20–7.35 (m, 5H); ^{13}C NMR (100 MHz, $CDCl_3$) δ 31.8, 34.9, 51.8, 62.7, 62.8, 71.1, 82.0, 126.8, 128.0, 128.9, 138.0]. To a solution of compound **9** (475 mg, 2.1 mmol) and quinoline **8** (387 mg, 1.5 mmol) in CH_2Cl_2 (12 mL), was added Et_3N (0.84 mL, 6.0 mmol) at rt. After being stirred overnight, the mixture was quenched with aqueous saturated $NaHCO_3$. The product was extracted with CH_2Cl_2. The organic layer was dried over Mg_2SO_4 and concentrated *in vacuo*. The product was purified by column chromatography (SiO_2, hexane/AcOE by increasing the gradient from 5:1 to 3:1 v/v). Further purification was achieved by recrystallization (hexane/AcOEt = 1:1) to give compound **DPH1** (196 mg, 33.8%) as a white solid: mp 145.5 °C; IR (KBr) ν 3289, 2958, 2914, 2805, 2754, 1582, 1510, 1422, 1360, 1281, 1229, 1186, 1152, 1107, 1069, 1001 cm^{-1}; ^{1}H NMR (400 MHz, $CDCl_3$) δ 1.60–1.76 (m, 2H), 1.90–2.02 (m, 4H), 2.17 (t, J = 2.3 Hz, 1H), 2.48–2.60 (m, 1H), 2.91 (d, J = 11.5 Hz, 2H), 3.16 (d, J = 2.3 Hz, 2H), 3.46 (s, 2H), 4.00 (s, 2H), 7.00 (d, J = 7.6 Hz, 1H), 7.15–7.29 (m, 5H), 7.31–7.40 (m, 2H), 8.60 (dd, J = 8.5, 1.6 Hz, 1H), 8.69 (dd, J = 4.3, 1.5 Hz, 1H) (the O*H* signal was not detected); ^{13}C NMR (100 MHz, $CDCl_3$) δ 29.6, 38.0, 51.3, 53.0, 58.5, 63.0, 73.1, 80.0, 108.8, 121.4, 124.9, 127.1, 127.7, 128.2 (2C), 129.2, 129.3, 133.9, 138.7, 147.5, 151.8. Anal. Calcd. for $C_{25}H_{27}N_3O$: C, 77.89; H, 7.06; N, 10.90. Found: C, 77.88; H, 7.10; N, 10.89.

4.1.4. 2-(1-Benzylpiperidin-4-yl)-2-(((8-hydroxyquinolin-5-yl) methyl)(prop-2-yny)amino)acetonitrile (DPH2)

To a cooled solution of 1-benzyl-4-piperidinecarboxaldehyde [58] (407 mg, 2.0 mmol) and propargylamine (165 mg, 3.0 mmol) in MeOH (6 mL) at 0 °C, a small amount of CF_3CO_2H (5 drops) was added. After being stirred for 1 h, $NaBH_3CN$ (189 mg, 2.9 mmol) was added to the solution portionwise. The mixture was stirred at rt overnight and then quenched with aqueous saturated $NaHCO_3$. The mixture was concentrated *in vacuo* and then extracted with AcOEt. The combined organic layers were dried over $MgSO_4$ and concentrated under reduced pressure to give a mixture that was purified by column chromatography (SiO_2, eluting solvent was changed from hexane/AcOEt = 5:1 to AcOEt and then AcOEt/MeOH = 4:1 v/v) to give *N*-[(1-benzylpiperidin-4-yl)methyl]prop-2-yn-1-amine (**10**) (232 mg, 50.2%), as an orange oil [R_f = 0.23 (AcOEt/MeOH = 4:1); IR (film) ν 3287, 3028, 2918, 2801, 2758, 1495, 1454, 1366, 1342, 1121, 1078 cm^{-1}; ^{1}H NMR (400 MHz, $CDCl_3$) δ 1.15–1.55 (m, 3H), 1.72 (d, J = 12.5 Hz, 2H), 1.95–2.11 (m, 2H), 2.20 (t, J = 2.3 Hz, 1H), 2.57 (d, J = 6.6 Hz, 2H), 2.94 (d, J = 11.7 Hz, 2H), 3.33–3.65 (m, 4H), 7.19–7.40 (m, 5H) (the N*H* signal was not observed); ^{13}C NMR (100 MHz, $CDCl_3$) δ 30.1, 35.8, 38.4, 53.4, 54.5, 63.1, 71.4, 82.2, 127.3, 128.3, 129.4, 137.3], and (1-benzylpiperidin-4-yl)(prop-2-yn-1-ylamino)acetonitrile (**11**) (165 mg, 30.9%) as an orange oil [R_f = 0.78 (AcOEt/MeOH = 4:1); IR (film) ν 3296, 2940, 2920, 2803, 2760, 1732, 1452, 1368, 1246, 1223, 1072 cm^{-1}; ^{1}H NMR (400 MHz, $CDCl_3$) δ 1.37–1.72 (m, 4H), 1.76–1.88 (m, 2H), 1.92–2.02 (m, 2H), 2.26–2.33 (m, 1H), 2.87–2.98 (m, 2H), 3.44–3.69 (m, 5H), 7.17–7.44 (m, 5H); ^{13}C NMR (100 MHz, $CDCl_3$) δ 28.4, 29.0, 36.8, 39.0, 53.0, 54.5, 63.0, 72.8, 80.1, 118.7, 127.1, 128.2, 129.1, 138.3].

To a solution of compound **11** (70 mg, 0.29 mmol) and Et_3N (0.085 mL, 0.58 mmol) in CH_2Cl_2 (2 mL), chloride **8** (70 mg, 0.25 mmol) was added. After stirring for 30 min at rt, brine was added to the mixture. The product was extracted with CH_2Cl_2, the extract was dried over Mg_2SO_4 and then concentrated *in vacuo*. The crude product was purified by column chromatography (hexane/AcOEtby increasing the gradient from 5:1 to 1:1 v/v), to give compound **DPH2** (99 mg, 80.6%) as a white solid: IR (KBr) ν 3443, 3300, 3026, 2949, 2814, 1580, 1504, 1476, 1454, 1424, 1371, 1269, 1229, 1193, 1150, 1072 cm^{-1}; ^{1}H NMR (600 MHz, $CDCl_3$) δ 0.68–0.70 (m, 1H), 1.17–1.22 (m, 1H), 1.65–1.95 (m, 5H), 2.41 (s, 1H), 2.65 (s, 1H), 2.81–2.83 (m, 1H), 3.23–3.29 (m, 3H), 3.34 (s, 1H), 3.45–3.48 (m, 1H), 3.68 (d, J = 13.2 Hz, 1H), 4.63 (d, J = 13.8 Hz, 1H), 7.1–7.20 (m, 1H), 7.21–7.28 (m, 5H), 7.40–7.44 (m, 2H), 8.60 (d, J = 8.4 Hz, 1H), 8.76 (d, J = 4.2 Hz, 1H) (the signal for O*H* was not detected); ^{13}C NMR (150 MHz, $CDCl_3$) δ 29.4, 30.7, 36.0, 40.0, 52.5, 54.2, 57.7, 63.1, 74.0, 78.8, 84.7, 108.9, 111.8, 116.0, 121.7, 122.2, 127.2, 127.5, 128.2, 129.3, 130.0, 134.0, 138.8, 148.9, 152.6. Anal. Calcd for $C_{27}H_{28}N_4O$: C, 76.39; H, 6.65; N, 13.20. Found: C, 76.45; H, 6.75; N, 13.17.

4.1.5. 5-((((1-Benzylpiperidin-4-yl)methyl)(prop-2-ynyl)amino) methyl)quinolin-8-ol (DPH3)

To a stirring solution of compound **10** (638 mg, 2.6 mmol) and chloride **8** (694 mg, 2.7 mmol) in CH_2Cl_2 (12 mL), Et_3N (1.09 mL, 5.2 mmol) was added at rt. After being stirred overnight, the mixture was quenched with water and the product was extracted with CH_2Cl_2, dried over Mg_2SO_4, concentrated *in vacuo*, and purified by column chromatography (SiO_2, hexane/AcOEt by increasing the gradient from 5:1 to 1:1 v/v) to give amine **DPH3** (572 mg, 55%) as a light brown solid: mp 128.5 °C; IR (KBr) ν 3320, 3248, 2946, 2914, 2754, 2365, 1734, 1580, 1506, 1478, 1422, 1366, 1279, 1229,

1192, 1128, 1065 cm^{-1}; ^1H NMR (400 MHz, $CDCl_3$) δ 0.97–1.14 (m, 2H), 1.32–1.48 (m, 1H), 1.60 (d, J = 12.5 Hz, 2H), 1.84 (t, J = 11.0 Hz, 2H), 2.19 (s, 1H), 2.36 (d, J = 7.2 Hz, 2H), 2.76 (d, J = 11.1 Hz, 2H), 3.15 (d, J = 1.9 Hz, 2H), 3.39 (s, 2H), 3.83 (s, 2H), 6.98 (d, J = 7.8 Hz, 1H), 7.12–7.37 (m, 7H), 8.53 (dd, J = 8.5, 1.4 Hz, 1H), 8.68 (dd, J = 4.2, 1.4 Hz, 1H) (the signal for O*H* was not detected); ^{13}C NMR (100 MHz, $CDCl_3$) δ 30.8, 33.5, 40.8, 53.6, 56.6, 59.1, 63.5, 73.4, 78.4, 108.7, 121.3, 124.9, 126.9, 127.8, 128.1, 129.1, 129.2, 134.1, 138.5, 138.7, 147.5, 151.9. Anal. Calcd for $C_{26}H_{29}N_3O$: C, 78.16; H, 7.32; N, 10.52. Found; C, 78.05; H, 7.36; N, 10.40.

4.1.6. (1-Benzylpiperidin-4-ylidene)acetonitrile (**12**) [59]

A solution of diethyl (cyanomethyl)phosphonate (2.13 g, 12 mmol) [prepared by heating triethylphosphite (1.0 equiv) and chloroacetonitrile (1.0 equiv) at 150 °C for 3.5 h; the crude product was directly used in the next reaction] and K_2CO_3 (1.39 g, 10 mmol) in dry THF (5 mL) was stirred for 15 min at rt. Then the mixture was heated to reflux for 20 min. After cooling down to rt, 1-benzyl-4-piperidone (1.90 g, 10 mmol) was added dropwise to this solution. Then the mixture was heated at reflux for 12 h. After cooling down to rt, 10% K_2CO_3 aqueous solution was added. The reaction mixture was extracted with AcOEt, and the organic layers were dried over $MgSO_4$ and concentrated *in vacuo* to give the crude product **12** (2.7 g, >99.0%), which was directly used in next step.

4.1.7. (1-Benzylpiperidin-4-yl)acetonitrile (**13**) [60]

To a solution of nitrile **12** (2.7 g, 10 mmol) in MeOH (100 mL), Mg (4.6 g, 191 mmol) and infinitesimal quantity of I_2 was added. The mixture was stirred until it became gray gel. After conc. HCl was added, the mixture became clear solution. Then it was treated with 10 N NaOH to alkaline. The precipitate was filtered and washed with large amount of EtOAc. The filtrate was extracted with AcOEt, and the combined organic layers were dried over $MgSO_4$ and concentrated *in vacuo* to give the product **13** (1.59 g, 74.5%).

4.1.8. (1-Benzylpiperidin-4-yl)acetaldehyde (**14**) [61]

To an oven-dried and argon-purged flask were added the nitrile **13** (1.29 g, 6.0 mmol) and THF (13 mL). The mixture was cooled to −78 °C, and DIBAL-H (6.22 mL, 1 mmol/mL) was added to the reaction *via* syringe. The reaction was stirred at −78 °C for 1 h, and then quenched with aqueous saturated $NaHCO_3$. The precipitate was filtered and washed with large amount of EtOAc. The filtrate was extracted with EtOAc. The combined organic layers were washed with brine and dried over $MgSO_4$. After concentrated in vacuum, the crude product was purified by chromatography (SiO_2, CH_2Cl_2/MeOH = 20:1 v/v) to give product **10** (365 mg, 27.8%).

4.1.9. 3-(1-Benzylpiperidin-4-yl)-2-(((8-hydroxyquinolin-5-yl) methyl)(prop-2-ynyl)amino)propanenitrile (DPH4)

A solution of **14** (365 mg, 1.68 mmol) and propargylamine (187 mg, 3.4 mmol) in MeOH (10 mL) was stirred at 0 °C for 1 h; then $NaBH_3CN$ (214 mg, 3.4 mmol) was added. The mixture was stirred at rt overnight. Water was added to the mixture and MeOH was removed under reduced pressure. Then aqueous saturated $NaHCO_3$ was added, and the mixture was extracted with AcOEt. The separated organic layers were dried over $MgSO_4$ and concentrated *in vacuo* to give the crude product. Further purification was achieved by column chromatography (SiO_2, eluting solvent was changed with gradient from hexane/AcOEt 5:1 to 1:5v/v and then change from AcOEt to AcOEt/MeOH 4:1 v/v) to give *N*-[2-(1-benzylpiperidin-4-yl)ethyl]prop-2-yn-1-amine (**15**) (168 mg, 38.9%), as an orange oil [R_f = 0.11 (MeOH/AcOEt = 1:4); IR (film) ν 3302, 2922, 2945, 2801, 2758, 1493, 1454, 1366, 1148, 1121, 1078, 1028 cm^{-1}; ^1H NMR (400 MHz, $CDCl_3$) δ 1.15–1.45 (m, 5H), 1.61 (d, J = 10.5 Hz, 2H), 1.94 (t, J = 11.1 Hz, 2H), 2.13 (t, J = 2.1 Hz, 1H), 2.63 (t, J = 7.2 Hz, 2H), 2.84 (d, J = 11.5 Hz, 2H), 3.30–3.55 (m, 4H), 7.12–7.33 (m, 5H) (the N*H* signal was not observed); ^{13}C NMR (100 MHz, $CDCl_3$) δ 32.0, 33.3, 36.3, 38.0, 45.9, 53.5, 63.1, 71.2, 82.0, 127.0, 128.0 (2C), 129.2 (2C), 137.5], and 3-(1-benzylpiperidin-4-yl)-2-(prop-2-yn-1-ylamino)propanenitrile (**16**) (190 mg, 40.2%) as an orange oil [R_f = 0.56 (MeOH/AcOEt = 1:4); IR (film) ν 3295, 2924, 2905, 2782, 1493, 1452, 1388, 1343, 1125, 1074 cm^{-1}; ^1H NMR (400 MHz, $CDCl_3$) δ 1.15–1.38 (m, 2H), 1.43–1.73 (m, 5H), 1.92 (t, J = 11.5 Hz, 2H), 2.21 (t, J = 2.3 Hz, 1H), 2.82 (d, J = 10.7 Hz, 2H), 3.35–3.64 (m, 4H), 3.66–3.78 (m, 1H), 7.13–7.33 (m, 5H) (the N*H* signal was not observed); ^{13}C NMR (100 MHz, $CDCl_3$) δ 31.7, 31.8, 32.2, 36.4, 39.9, 46.9, 53.2, 63.2, 72.7, 79.8 (2C), 119.6, 126.9, 128.0 (2C), 129.0 (2C), 138.1].

To a cooled mixture of **16** (84 mg, 0.3 mmol) and Et_3N (0.093 mL, 0.67 mmol) in CH_2Cl_2 (6 mL), chloride **8** (77 mg, 0.3 mmol) was added at 0 °C. After being stirred at rt overnight, the reaction was quenched with aqueous 5% $NaHCO_3$. The reaction mixture was extracted with CH_2Cl_2, and extracts were dried with Mg_2SO_4 and concentrated *in vacuo*. The crude product was purified by column chromatography (hexane: AcOEt by increasing the gradient from 5:1 to 1:1 v/v) to give compound **DPH4** (91.4 mg, 69.5%) as an orange oil: IR (film) ν 3298, 2934, 2807, 1580, 1505, 1476, 1370, 1273, 1233, 1198, 1148, 1072, 1028 cm^{-1}; ^1H NMR (400 MHz, $CDCl_3$) δ 0.81–0.93 (m, 1H), 0.93–1.07 (m, 1H), 1.12–1.32 (m, 2H), 1.38–1.62 (m, 3H), 1.69 (ddd, J = 14.1, 8.8, 5.5 Hz, 1H), 1.76–1.89 (m, 1H), 2.39–2.47 (m, 1H), 2.58 (d, J = 11.3 Hz, 1H), 2.80 (d, J = 11.5 Hz, 1H), 3.21–3.32 (m, 1H), 3.36–3.53 (m, 3H), 3.65–3.75 (m, 2H), 4.60 (d, J = 13.1 Hz, 1H), 7.06–7.11 (m, 1H), 7.21–7.33 (m, 5H), 7.40–7.47 (m, 2H), 8.58–8.65 (m, 1H), 8.75–8.81 (m, 1H) (the signal for O*H* was not detected); ^{13}C NMR (100 MHz, $CDCl_3$) δ 30.6, 31.5, 37.2, 39.8, 49.6, 52.7, 53.0, 53.6, 62.8, 74.1, 78.6, 108.9, 117.0, 121.6, 122.3, 127.2, 127.5, 128.1, 129.3, 129.8, 133.6, 138.6, 147.7, 152.5. HRMS. Calcd. for $C_{28}H_{31}N_4O$ $(M + H)^+$: 439.2428. Found: 439.2532 $(M + H)^+$.

4.1.10. 5-(((2-(1-Benzylpiperidin-4-yl)ethyl)(prop-2-ynyl)amino) methyl)quinolin-8-ol (DPH5)

To a cooled mixture of **15** (46 mg, 0.18 mmol) and Et_3N (0.053 mL, 0.38 mmol) in CH_2Cl_2 (2.5 mL) at 0 °C, chloride **8** (47 mg, 0.18 mmol) was added. After being stirred at rt overnight, the reaction was quenched with aqueous 5% $NaHCO_3$. The product was extracted with CH_2Cl_2, and extracts were dried over Mg_2SO_4 and then concentrated *in vacuo*. The crude product was purified by column chromatography (hexane/AcOE tby increasing the gradient from 5:1 to 1:1 v/v) to give compound **DPH5** (40 mg, 53.5%) as a yellow oil: IR (film) ν 3254, 2945, 2915, 2805, 2758, 1578, 1508, 1478, 1420, 1375, 1350, 1279, 1231, 1194, 1148, 1121 cm^{-1}; ^1H NMR (400 MHz, $CDCl_3$) δ 1.24 (s, 3H), 1.44 (d, J = 33.20 Hz, 4H), 1.82 (m, 2H), 2.67 (t, J = 2.40 Hz, 1H), 2.58 (t, J = 7.20 Hz, 2H), 2.83 (d, J = 11.20 Hz, 2H), 3.26 (d, J = 2.40 Hz, 2H), 3.48 (s, 2H), 3.92 (s, 2H), 7.08 (d, J = 8.00 Hz, 1H), 7.30–7.44 (m, 7H), 8.61–8.61 (m, 1H), 8.76–8.77 (m, 1H) (the signal for O*H* was not detected); ^{13}C NMR (100 MHz, $CDCl_3$) δ 32.2, 33.5, 33.9, 41.0, 50.3, 53.7, 55.9, 63.3, 72.3, 78.3, 108.7, 121.4, 124.9, 127.0, 127.9, 128.1, 129.2, 129.3, 134.0, 138.7, 147.5, 151.8. HRMS. Calcd. for $C_{27}H_{32}N_3O$ $(M + H)^+$: 414.2545. Found: 414.2570 $(M + H)^+$.

4.1.11. (2E)-3-(1-benzylpiperidin-4-yl)prop-2-enenitrile (**17**) [62]

A mixture of diethyl (cyanomethyl)phosphonate (2.2 g, 12 mmol) and K_2CO_3 (1.4 g, 10 mmol) in dry THF (100 mL) was stirred at rt for 15 min, and then heated at reflux for 20 min. After cooling down to rt, 1-benzyl-4-piperidinecarboxaldehyde [58] (2.0 g, 10 mmol) was added. The mixture was heated to reflux for 3 h. Aqueous 10% K_2CO_3 water (100 mL) was added after cooling down to rt. The product was extracted with AcOEt and dried over $MgSO_4$. After concentrated *in vacuum*, the crude product was

purified by column chromatography (SiO_2, hexane/AcOEt from 5:1 to 1:1 v/v) to give nitrile **17** (0.74 g, 32.6%).

4.1.12. 3-(1-Benzylpiperidin-4-yl)propanenitrile (**18**) [63]

To a solution of **17** (1.74 g, 7.70 mmol) in MeOH (33 mL) at rt, turning of Mg (3.70 g, 154 mmol) and infinitesimal quantity of I_2 was added to the mixture. The mixture was stirred until it became gray gel. After conc. HCl was added, the mixture became clear solution. Then it was treated with 10 N NaOH to alkaline. The precipitates were filtered and washed with large amount of EtOAc. The filtrate was extracted with AcOEt, and the combined organic layers were dried over $MgSO_4$ and concentrated *in vacuo* to give the crude product **18** (1.76 g, 99.9%).

4.1.13. 3-(1-Benzylpiperidin-4-yl)propanal (**19**) [64]

To an oven-dried and argon-purged flask were added the nitrile **18** (1.00 g, 4.4 mmol) and THF (10 mL). The reaction was cooled to −78 °C, and DIBAL-H (4.54 mL, 1 mmol/mL) was added to the reaction *via* syringe. The mixture was stirred at −78 °C for 1 h, and then quenched with aqueous saturated $NaHCO_3$. The precipitates were filtered and washed with large amount of EtOAc. The filtrate was extracted with EtOAc. The combined organic layers were washed with brine and dried over $MgSO_4$. After concentrated in vacuum, the crude product was purified by chromatography (SiO_2, CH_2Cl_2/MeOH = 20:1 v/v), to give aldehyde **19** (427 mg, 42.7%).

4.1.14. 4-(1-Benzylpiperidin-4-yl)-2-(((8-hydroxyquinolin-5-yl)methyl)(prop-2-yny)amino)butanenitrile (DPH6)

A solution of aldehyde **19** (427 mg, 1.9 mmol) and propargylamine (204 mg, 3.7 mmol) in MeOH (6 mL) was stirred at 0 °C for 1 h, then $NaBH_3CN$ (1.3 g, 2.0 mmol) was added. The mixture was stirred at rt overnight. Water was added to the mixture and MeOH was removed under reduced pressure. Then, aqueous saturated $NaHCO_3$ was added, and the mixture was extracted with AcOEt. The separated organic layers were dried over $MgSO_4$ and concentrated *in vacuo* to give the crude products. Further purification was achieved by column chromatography (SiO_2, eluting solvent was changed with gradient from hexane/AcOEt 5:1 to 1:5v/v and then change from AcOEt to AcOEt/MeOH 4:1 v/v) to give *N*-[3-(1-benzylpiperidin-4-yl)propyl]prop-2-yn-1-amine (**20**) (221 mg, 44.2%), as a yellow oil [R_f = 0.19 (MeOH/AcOEt = 1:4); IR (film) ν 3304, 3028, 2922, 2847, 2794, 2758, 1495, 1452, 1386, 1343, 1119, 1028 cm^{-1}; ^1H NMR (600 MHz, $CDCl_3$) δ 1.10–1.26 (m, 5H), 1.33–1.46 (m, 2H), 1.58 (d, J = 9.9 Hz, 2H), 1.87 (br s, 2H), 2.13 (t, J = 2.3 Hz, 1H), 2.31–2.39 (m, 1H), 2.59 (t, J = 7.1 Hz, 1H), 2.81 (d, J = 10.8 Hz, 2H), 3.35 (d, J = 2.3 Hz, 2H), 3.43 (s, 2H), 7.13–7.29 (m, 5H) (the N*H* signal was not observed); ^{13}C NMR (150 MHz, $CDCl_3$) δ 24.6, 27.0, 32.2, 32.3, 34.1, 35.6, 38.0, 48.8, 53.8, 63.4, 71.1, 82.2, 126.7, 128.0, 129.1, 138.4], and 4-(1-benzylpiperidin-4-yl)-2-(prop-2-yn-1-ylamino)butanenitrile (**21**) (234 mg, 42.7%), as an yellow oil [R_f = 0.59 (MeOH/AcOEt = 1:4); IR (film) ν 3296, 2911, 2845, 2801, 2780, 1493, 1452, 1368, 1343, 1312, 1260, 1146, 1119, 1074; ^1H NMR (400 MHz, $CDCl_3$) δ 1.18–1.69 (m, 8H), 1.70–1.83 (m, 2H), 1.85–2.02 (m, 2H), 2.23–2.37 (m, 1H), 2.87 (d, J = 10.5 Hz, 2H), 3.29–3.76 (m, 4H), 7.16–7.38 (m, 5H) (the N*H* signal was not observed); ^{13}C NMR (100 MHz, $CDCl_3$) δ 31.0, 31.6, 32.1, 32.2, 32.3, 35.4, 36.6, 49.5, 53.7, 63.4, 72.8, 80.0, 119.4, 126.7, 127.9, 128.9, 138.1].

To a mixture of amine **21** (89 mg, 0.3 mmol) and Et_3N (0.09 mL, 0.7 mmol) in CH_2Cl_2 (6 mL) at 0 °C, chloride **8** (77 mg, 0.3 mmol) was added. After being stirred at rt overnight, the reaction was quenched with aqueous 5% $NaHCO_3$ and the product was extracted with CH_2Cl_2. The extracts were dried Mg_2SO_4, and concentrated *in vacuo*. The crude products were purified by column chromatography (SiO_2, hexane/AcOEt by increasing the gradient from 5:1 to 1:1 v/v), to give compound **DPH6** (89 mg, 65.4%) as a yellow oil: IR (film) ν 3295, 2931, 2812, 1578, 1505, 1476, 1371, 1271, 1203, 1196, 1148, 1123, 1072, 1028 cm^{-1}; ^1H NMR (400 MHz, $CDCl_3$) δ 0.99–0.77 (m, 1H), 1.40–1.38 (m, 6H), 1.53–1.40 (m, 1H), 1.84–1.60 (m, 5H), 2.42 (t, J = 2.4 Hz, 1H), 2.77 (ddt, J = 12.0, 8.3, 2.1 Hz, 1H), 3.28 (dd, J = 16.8, 2.4 Hz, 1H), 3.45 (s, 2H), 3.58 (dd, J = 16.8, 2.4 Hz, 1H), 3.75 (d, J = 13.1 Hz, 1H), 4.60 (d, J = 13.1 Hz, 1H), 7.11 (d, J = 7.6 Hz, 1H), 7.32–7.22 (m, 5H), 7.57–7.39 (m, 2H), 8.64 (dd, J = 8.5, 1.6 Hz, 1H), 8.78–8.80 (m, 1H) (the signal for O*H* was not detected); ^{13}C NMR (100 MHz, $CDCl_3$) δ 28.1, 31.5, 31.9, 32.0, 34.4, 39.8, 52.3, 53.4, 53.5, 53.7, 63.3, 74.2, 78.6, 108.9, 117.2, 121.8, 122.5, 127.1, 127.6, 128.2, 129.3, 129.9, 133.7, 138.8, 147.9, 152.6. HRMS. Calcd for $C_{29}H_{33}N_4O$ $(M + H)^+$: 453.2654. Found: 452.2526 $(M + H)^+$.

4.1.15. 5-(((3-(1-Benzylpiperidin-4-yl)propyl)(prop-2-ynyl)amino)methyl)quinolin-8-ol (DPH7)

To a cooled mixture of amine **20** (189 mg, 0.70 mmol) and Et_3N (0.51 mL, 2.5 mmol) in CH_2Cl_2 (15 mL) at 0 °C, chloride **8** (186 mg, 0.73 mmol) was added. After being stirred at rt overnight, the reaction was quenched with aqueous 5% $NaHCO_3$. The product was extracted with CH_2Cl_2, and extracts were dried over Mg_2SO_4 and then concentrated *in vacuo*. The crude products were purified by column chromatography (SiO_2, hexane/AcOEt by increasing the gradient from 5:1 to 1:1 v/v) to give compound **DPH7** (162 mg, 54.3%) as a yellow oil: IR (film) ν 3381, 3293, 2911, 2801, 1738, 1580, 1505, 1476, 1425, 1373, 1289, 1238, 1198, 1047 cm^{-1}; ^1H NMR (300 MHz, $CDCl_3$) δ 0.99–1.33 (m, 5H), 1.42–1.66 (m, 4H), 1.86 (t, J = 11.3 Hz, 2H), 2.29 (t, J = 2.1 Hz, 1H), 2.56 (t, J = 7.1 Hz, 2H), 2.86 (d, J = 11.4 Hz, 2H), 3.26 (d, J = 2.2 Hz, 2H), 3.48 (s, 2H), 3.93 (s, 2H), 7.09 (d, J = 7.6 Hz, 1H), 7.20–7.37 (m, 5H), 7.37–7.49 (m, 2H), 8.65 (dd, J = 8.5, 1.3 Hz, 1H), 8.77 (dd, J = 4.1, 1.3 Hz, 1H) (the signal for O*H* was not detected); ^{13}C NMR (100 MHz, $CDCl_3$) δ 24.4, 32.2, 34.0, 35.3, 40.9, 53.2, 53.8 (2C), 55.8, 63.4, 73.4, 78.4, 108.9, 121.4, 124.9, 127.0, 127.9, 128.2, 129.2, 129.3, 134.1, 138.7, 147.6, 152.0. Anal. Calcd for $C_{28}H_{33}N_3O$: C, 78.65; H, 7.78; N, 9.83. Found; C, 76.90; H, 8.03; N 9.98.

4.1.16. 4-(1-Benzylpiperidin-4-yl)-2-(prop-2-yn-1-ylamino)butanenitrile (**21**)

3-(1-Benzylpiperidin-4-yl)propanal (**19**) (136 mg, 0.59 mmol), prop-2-yn-1-amine (47 μL, 0.74 mmol, 1.25 equiv) and trimethylsilyl cyanide (TMSCN) (0.14 mL, 1.1 mmol, 1.85 equiv) were mixed and submitted to microwave irradiation at 125 °C for 10 min. The crude reaction was purified by column chromatography (SiO_2, hexane/AcOEt from 9:1 to 1:1 v/v) to give compound **21** (104 mg, 60%) as a yellow oil, that showed identical spectroscopic data to the compound isolated in the Mannich reductive amination of aldehyde **19**. α-Aminonitrile **21** was also transformed into target compound **DPH6** (see above).

4.2. Pharmacological evaluation

4.2.1. Cholinesterase inhibition

Cholinesterase activities were assessed following a spectrophometric method [18], using purified AChE from *Electrophorus electricus* (type V–S) and purified BuChE from equine serum (lyophilized powder) (Sigma–Aldrich, Madrid, Spain). Enzymatic reactions took place in 96-well plates in solutions containing 0.1 M phosphate buffer (pH 8.0), 0.035 U/mL AChE or 0.05 U/mL BuChE and 0.35 mM of 5,5′-dithiobis-2-nitrobenzoic acid (DTNB, Sigma–Aldrich, Madrid, Spain). Inhibition curves were plotted by pre-incubating this mixture with serial dilutions of each compound for 20 min. The activity in absence of compounds was used to determine the 100% of enzyme activity. After pre-incubation times, 50 μl of substrate were added to a final concentration of 0.35 mM acetylthiocholine iodide or 0.5 mM butyrylthiocholine iodide

(Sigma–Aldrich). Enzymatic reactions were followed for 5 min with AChE or 25 min with BuChE. Changes in absorbance at λ_{405} in a spectrophotometic plate reader (FluoStar OPTIMA, BMG Labtech) were detected and IC_{50} values calculated at the compound concentration inhibiting 50% of enzymatic activity by using the GraphPad 'PRISM' software (version 3.0). Data were expressed as mean ± SEM of at least three different experiments performed in triplicate.

4.2.1.1. Kinetic studies of AChE inhibition by DHP6. To estimate the mechanism of action of DPH6 inhibiting AChE, reciprocal plots of 1/V versus 1/[S] were determined at different acetylthiocholine (ASCh) concentrations (0.1–5 μM). The plots were assessed by a weighted least-squares analysis. Slopes of reciprocal plots were plotted against concentration of DPH6 (0–5 μM) for AChE to determine the reversible inhibition constant (K_i).

4.2.2. Monoamine oxidase inhibition

To assess the inhibition of MAO A and MAO B by derivatives **DHPs 1–7**, ^{14}C-labeled substrates were used (Perkin Elmer, USA). Rat liver homogenates were used as source of MAO [19]. MAO A activity was determined using 100 μM (0.5 mCi/mmol) [^{14}-C]-(5-hydroxytryptamine) (5-HT) whereas MAO B activity was determined using 20 μM (2.5 mCi/mmol) [^{14}C]-phenylethylamine (PEA). Inhibition curves were plotted by pre-incubating the enzyme with several concentrations of each compound for 30 min in 50 mM phosphate buffer (pH 7.4). Inhibitor-free samples were used to determine the 100% of enzyme activity. At the end of each pre-incubation, substrate (25 μl) was added in a final volume of 225 μl and reactions allowed for 20 min (MAO A) or 4 min (MAO B). Reactions were stopped by adding 2 M citric acid and radiolabelled-aldehyde products extracted into toluene/ethylacetate (1:1, v/v) containing 0.6% (w/v) 2,5-diphenyloxazole prior to liquid scintillation counting (Tri-Carb 2810TR). Inhibition curves were plotted as previously mentioned. Total protein was measure by the method of Bradford (1976) using bovine-serum albumin as standard.

4.2.2.1. Reversibility and time-dependence of MAO by DHP6. The study of reversibility inhibition exerted by **DPH6** towards MAO A and MAO B were determined by incubating the enzyme in the presence and in the absence of the inhibitor before and after three consecutive washings with buffer. MAO A and MAO B samples were pre-incubated for 30 min at 37 °C with 10 μM **DPH6** and 20 μM **DPH6**, respectively. A sample of 50 nM clorgyline and 20 nM *l*-deprenyl was also used as control of irreversible MAO A and MAO B inhibition. Samples were washed with 50 mM phosphate buffer (pH 7.4) and centrifuged at 25,000 g for 10 min at 4 °C consecutively three times. Total protein was measured by the Bradford method and MAO activity determined as described above. Time-dependence inhibition of **DPH6** towards MAO A and MAO B was evaluated by pre-incubating varying concentrations of the inhibitor with the enzyme at different times (0–180 min). Dose-response curves (IC_{50}) values were accordingly determined for each time as described above.

4.2.3. Determination of metal-chelating properties

Complexing studies were performed in distilled water at room temperature using a UV–VIS spectrophotometer (Lambda25, PerkinElmer). Spectrums (220–300 nm) of DPH6 alone (10 μM) and in presence of varying concentrations of $CuSO_4$ (no changes observed after 5-min incubation), $Fe_2(SO)_3$ (no changes observed following O/N incubation) and $ZnSO_4$ (no changes observed after 1-h incubation) were recorded in 1 cm quartz cells. The stoichiometry of the complexes **DPH6**-Cu(II)/Zn(II)/Fe(III) was determined by the Job's method [65]. Series of different solutions containing **DPH6** and biometals $CuSO_4$, $ZnSO_4$ or $Fe_2(SO_4)_3$ were prepared at a final sum of concentrations of both species of 10 μM, varying the proportions of both components between 0 and 100%. Absorbance at 257 nm was plotted versus the mole fraction of DPH**6** for each metal.

4.2.4. Toxicity in human hepatoma cell line HepG2: culture of HepG2 liver cells and treatment

Human hepatoma cell line HepG2 was cultured in Eagle's minimum essential medium (EMEM) supplemented with 15 non-essential amino acids, 1 mM sodium pyruvate, 10% heat-inactivated fetal bovine serum (FBS), 100 units/mL penicillin, and 100 μg/mL streptomycin (reagents from Invitrogen, Madrid, Spain). Cells were seeded into flasks containing supplemented medium and maintained at 37 °C in a humidified atmosphere of 5% CO_2 and 95% air. For assays, HepG2 cells were subcultured in 96-well plates at seeding density of 8×10^4 cells per well. When HepG2 cells reached 80% confluence, the medium was replaced with fresh medium containing 1–1000 μM compounds or 0.1% DMSO as a vehicle control.

4.2.5. MTT assay and cell viability

Cell viability, virtually the mitochondrial activity of living cells, was measured by quantitative colorimetric assay with 3-[4,5 dimethylthiazol-2-yl]-2,5-diphenyl-tetrazolium bromide (MTT) (Sigma Aldrich), as described previously [51]. Briefly, 50 μl of the MTT labeling reagent, at a final concentration of 0.5 mg/ml, was added to each well at the end of the incubation time and the plate placed in a humidified incubator at 37 °C with 5% CO_2 and 95% air (v/v) for an additional 2 h period. Then, the insoluble formazan was dissolved with dimethylsulfoxide; colorimetric determination of MTT reduction was measured at 540 nm. Control cells treated with EMEM were used as 100% viability.

4.2.6. In vivo analysis: relief of scopolamine-induced long-term memory deficit in mice by DHP6

4.2.6.1. Animals. Thirty-six male C57BL/6J mice (Harlan), weighing 25 g served as subjects in order to obtain our results. Animals were housed under controlled light (with a 12-h light/12-h dark cycle, lights on at 7:00 a.m.). Procedures were carried out following the European Communities Council Directive (86/609/EEC) on animal experiments.

4.2.6.2. Drugs and treatments. Scopolamine hydrobromide, 1 mg/kg (Sigma, St. Louis, MO, USA), donepezil, 1 mg/kg (Tocris Bioscience, R&D Systems Inc., Minneapolis, USA), and DPH6 (35 mg/kg) were given in 10 ml/kg of saline solution (0.9% NaCl) by intraperitoneal *via*. Animals were divided into four experimental handling groups: mice administered with i) saline (vehicle, $n = 9$); ii) scopolamine (vehicle + scop, $n = 9$); iii) donepezil plus scopolamine (donepezil + scop, $n = 10$); and iv) DPH6 plus scopolamine (DPH6 + scop, $n = 8$).

4.2.6.3. Passive avoidance task. The test was performed using the Ugo Basile (Comerio, Italy) apparatus. Basically, the device consists of two compartments (10 × 13 × 15 cm) connected by a sliding door. One compartment is brightly lit (10 W) and, on the contrary, the other one is dark and equipped with an electrified grid floor. Rodents tend to prefer dark environments and will immediately enter the darkened compartment. The day before of the experiment, mice are placed in the experimental room for 1 h. The experiment is performed in two consecutive days. The first day, scopolamine or saline is administered 30 min before the training session and saline, donepezil or **DPH6** are administered 90 min prior to the administration of scopolamine or saline. During the training session, each mouse is individually placed in the

illuminated compartment with the sliding door closed. 30 sec later, the door is open so that the mouse can move freely to each room. Once the mouse gets into the dark compartment, the sliding door closes automatically and the animal receives an electric foot shock (0.5 mA, 1 s). Then, mice are returned their home cage and 24 h later, in the second day, the probe session takes place. In the second day, each individual is placed again into illuminated box. Then the sliding door opens for 5 s with the electric foot-shock switched off in the dark room. The latency in seconds taken by a mouse to enter the dark compartment after door opening during the training and the probe session was automatically determined by the computer device. A cut-off time of 5 min was defined.

4.2.6.4. Statistical analysis. Significance was determined using a one-way analysis of variance (ANOVA), followed by Bonferroni's post hoc test. Statistical analysis of differences within a group between training and probe sessions were determined by using the Student's t- test. These statistical analyses have been carried out by using GraphPad Prism 5 computer software. Results are expressed as the average of latencies ±S.E.M. Differences are considered statistically significant at $p < 0.05$.

4.2.7. Molecular modeling

4.2.7.1. Molecular docking into AChE and BuChE. (*R*)-**DPH6** and (*S*)-**DPH6** were assembled as hydrochlorides and free bases within Discovery Studio, version 2.1, software package, using standard bond lengths and bond angles. With the CHARMm force field [66] and partial atomic charges, the molecular geometries of (*R*)-**DPH6** and (*S*)-**DPH6** were energy-minimized using the adopted-based Newton–Raphson algorithm. Structures were considered fully optimized when the energy changes between iterations were less than 0.01 kcal/mol [67].

4.2.7.2. Molecular docking of (R)-DPH6 and (S)-DPH6 into EeAChE. The coordinates of *E. electricus* AChE (PDB ID: 1C2B), were obtained from the Protein Data Bank (PDB). For docking studies, initial protein was prepared by removing all water molecules, heteroatoms, any co-crystallized solvent and the ligand. Proper bonds, bond orders, hybridization and charges were assigned using protein model tool in Discovery Studio, version 2.1, software package. CHARMm force field was applied using the receptor–ligand interactions tool in Discovery Studio, version 2.1, software package. Docking calculations were performed with the program Autodock Vina [22]. AutoDockTools (ADT; version 1.5.4) was used to add hydrogens and partial charges for proteins and ligands using Gasteiger charges. Flexible torsions in the ligands were assigned with the AutoTors module, and the acyclic dihedral angles were allowed to rotate freely. Trp286, Tyr124, Tyr337, Tyr72, Asp74, Thr75, Trp86, and Tyr341 receptor residues were selected to keep flexible during docking simulation using the AutoTors module. Because VINA uses rectangular boxes for the binding site, the box center was defined and the docking box was displayed using ADT. For *E. electricus* AChE (PDB ID: 1C2B) the docking procedure was applied to whole protein target, without imposing the binding site ("blind docking"). A grid box of $60 \times 60 \times 72$ with grid points separated 1 Å, was positioned at the middle of the protein ($x = 21.5911$; $y = 87.752$; $z = 23.591$). Default parameters were used except num_modes, which was set to 40. The AutoDock Vina docking procedure used was previously validated [23].

4.2.7.3. Molecular docking of inhibitors (R)-DPH6 and (S)-DPH6 into eqBuChE. The horse BuChE model has been retrieved from the SWISS-MODEL Repository. This is a database of annotated three-dimensional comparative protein structure models generated by the fully automated homology-modeling pipeline SWISS-MODEL. A putative three-dimensional structure of eqBuChE has been created based on the crystal structure of *h*BuChE (PDB ID: 2PM8), these two enzyme exhibited 89% sequence identity. Proper bonds, bond orders, hybridization and charges were assigned using protein model tool in Discovery Studio, version 2.1, software package. CHARMm force field was applied using the receptor–ligand interactions tool in Discovery Studio, version 2.1, software package. Docking calculations were performed following the same protocol described before for *Ee*AChE. All dockings were performed as blinds dockings where a cube of 75 Å with grid points separated 1 Å, was positioned at the middle of the protein ($x = 29.885$; $y = -54.992$; $z = 58.141$). Default parameters were used except num_modes, which was set to 40. The lowest docking-energy conformation was considered as the most stable orientation. Finally, the docking results generated were directly loaded into Discovery Studio, version 2.1.

4.2.7.4. Molecular docking of compounds (R)-DPH6 and (R)-DPH7 into rat MAO A/B. Compounds (*R*)-**DPH6** and (*R*)-**DPH7** were assembled as non-protonated amine within Discovery Studio, version 2.1, software package, following the procedure described before for cholinesterases. The crystal structure of rat MAO A in complex with its irreversible inhibitor MLG-709 was obtained from the Protein Data Bank (PDB ID 1O5W). The rat MAO B model has been retrieved from the SWISS-MODEL Repository. A putative three-dimensional structure of rat MAO B has been created based on the crystal structure of hMAO B (PDB ID: 1S3E), these two enzymes exhibited 89% sequence identity. For docking studies initial proteins were prepared. First, in the PDB crystallographic structure 1O5W (rat MAO A), any co-crystallized solvent and the ligand were removed; it is not necessary in the PDB MAO B model. Then, proper bonds, bond orders, hybridization and charges were assigned using protein model tool in Discovery Studio, version 2.1, software package. CHARMm force field was applied using the receptor–ligand interactions tool in Discovery Studio, version 2.1, software package. Six water molecules located around the FAD cofactor were considered in the docking experiments because of their well-known role into the MAO's inhibition. Finally, atoms of the FAD cofactor were defined in their oxidized state. Docking calculations were performed following the same protocol described before for *Ee*AChE. In docking with MAO A, Tyr 69, Leu97, Gln99, Ala111, Phe112, Tyr124, Trp128, Phe173, Leu176, Phe177, Ile180, Asn181, Ile207, Phe208, Gln215, Cys323, Ileu325, Ileu335, Phe352, Tyr407 and Tyr444 receptor residues were selected to keep flexible during docking simulation using the AutoTors module. All dockings were performed as blind dockings where a cube of 40 Å with grid points separated 1 Å, was centered on the FAD N5. Default parameters were used except num_modes, which was set to 40. According to Vina best scored poses, the most stable complex configurations were considered. At the end of the docking, the best poses were analyzed using Discovery Studio.

4.3. Statistical analysis

Significance was determined using a one-way analysis of variance (ANOVA), followed by Bonferroni's post hoc test. Significant differences within group were determined with the Student's *t*-test. Results are expressed as the average of latencies ± S.E.M. Differences are considered statistically significant at $p < 0.05$.

Acknowledgments

Supported by MINECO (SAF2012-33304 to JMC; to SAF2010-15173 RMM), MICINN for a grant (CTQ2009-10478 to ES), and EU (COST Action CM1103). Oscar M. Bautista-Aguilerta thanks MINECO

(Spain) for a FPI fellowship. G.E. and L.W have equally contributed to this work.

Appendix A. Supplementary data

Supplementary data related to this article can be found at http://dx.doi.org/10.1016/j.ejmech.2014.04.078.

References

[1] M. Goedert, M.G. Spillantini, Science 314 (2006) 777–781.
[2] A. Castro, A. Martínez, Current Pharmaceutical Design 12 (2006) 4377–4387.
[3] A. Gella, N. Durany, Cell Adhesion & Migration 3 (2009) 88–93.
[4] C. Geula, M.M. Mesulam, Neuroscience 33 (1989) 469–481.
[5] E. Scarpini, P. Scheltens, H. Feldman, Lancet Neurology 2 (2003) 539–547.
[6] V.N. Talesa, Mechanisms of Ageing and Development 122 (2001) 1961–1969.
[7] A. Cavalli, M.L. Bolognesi, A. Minarini, M. Rosini, V. Tumiatti, M. Recanatini, C. Melchiorre, Journal of Medicinal Chemistry 51 (2008) 347–372.
[8] I. Bolea, J. Juárez-Jiménez, C. de los Ríos, M. Chioua, R. Pouplana, F.J. Luque, M. Unzeta, J. Marco-Contelles, A. Samadi, Journal of Medicinal Chemistry 54 (2011) 8251–8270.
[9] I. Bolea, A. Gella, L. Monjas, C. Perez, M.I. Rodríguez-Franco, J. Marco-Contelles, A. Samadi, M. Unzeta, Currrent Alzhimer Research 9 (2013) 797–808.
[10] J. Mitoma, A. Ito, Journal of Biochemistry 111 (1992) 20–24.
[11] T.P. Singer, Chemistry and Biochemistry of Flavoenzymes, F. Müller, (Ed.), CRC Press, Boca Ratón, FL, USA, vol. III, pp. 437–470.
[12] S.Y. Son, J. Ma, Y. Kondou, M. Yoshimura, E. Yamashita, T. Tsukihara, Proceedings of the National Academy of Sciences of the United States of America 105 (2008) 5739–5744.
[13] C. Binda, M. Li, F. Hubalek, N. Restelli, D.E. Edmondson, A. Mattevi, Proceedings of the National Academy of Sciences of the United States of America 100 (2003) 9750–9755.
[14] V. Pérez, J.L. Marco, E. Fernández-Alvarez, M. Unzeta, British Journal of Pharmacology 127 (1999) 869–876.
[15] Y. Avramovich-Tirosh, T. Amit, O. Bar-Am, H. Zheng, M. Fridkin, M.B.H. Youdim, Journal of Neurochemistry 100 (2007) 490–502.
[16] H. Zheng, M.B.H. Youdim, M. Fridkin, Journal of Medicinal Chemistry 52 (2009) 4095–4098.
[17] V. Moret, Y. Laras, T. Cresteil, G. Aubert, D.Q. Ping, C. Di, M. Barthélémy-Requin, C. Béclin, V. Peyrot, D. Allegro, A. Rolland, F. De Angelis, E. Gatti, Ph. Pierre, L. Pasquini, E. Petrucci, U. Testa, J.L. Kraus, European Journal of Medicinal Chemistry 44 (2009) 558–567.
[18] G.L. Ellman, K.D. Courtney, V. Andres, R.M. Featherstone, Biochemical Pharmacology 7 (1961) 88–95.
[19] C.J. Fowler, K.F. Tipton, Biochemical Pharmacology 30 (1981) 3329–3332.
[20] A. Ozaita, G. Olmos, M.A. Boronat, J.M. Lizcano, M. Unzeta, J.A. García-Sevilla, British Journal of Pharmacology 121 (1997) 901–912.
[21] X. Huang, M.P. Cuanjungco, C.S. Atwood, M.A. Hartshorn, J.D. Tyndall, G.R. Hanson, K.C. Stokes, M. Leopold, G. Multhaup, L.E. Goldstein, R.C. Scarpa, A.J. Saunders, J. Lim, R.D. Moir, C. Glabe, E.F. Bowden, C.L. Masters, D.P. Fairlie, R.E. Tanzi, A.I. Bush, The Journal of Biological Chemistry 274 (1999) 37111–37116.
[22] O. Trott, A.J. Olson, Journal of Computational Chemistry 31 (2010) 455–461.
[23] M. Bartolini, M. Pistolozzi, V. Andrisano, J. Egea, M.G. López, I. Iriepa, I. Moraleda, E. Gálvez, J.L. Marco-Contelles, A. Samadi, ChemMedChem 6 (2011) 1990–1997.
[24] C. Martins, M.C. Carreiras, R. Léon, C. de los Ríos, M. Bartolini, V. Andrisano, I. Iriepa, I. Moraleda, E. Gálvez, M.G. García, J. Egea, A. Samadi, M. Chioua, J.L. Marco-Contelles, European Journal of Medicinal Chemistry 46 (2011) 6119–6130.
[25] K. Arnold, L. Bordoli, J. Kopp, T. Schwede, Bioinformatics 22 (2006) 195–201.
[26] F. Kiefer, K. Arnold, M. Künzli, L. Bordoli, T. Schwede, Nucleic Acids Research 37 (2009) D387–D392.
[27] M.C. Peitsch, Bio/Technology 13 (1995) 658–660.
[28] C. Binda, P. Newton-Vinson, F. Hubalek, N. Restelli, D.E. Edmondson, A. Mattevi, Nature Structural & Molecular Biology 2 (2002) 22–26.
[29] A. Samadi, C. de los Ríos, I. Bolea, M. Chioua, I. Iriepa, I. Moraleda, M. Bartolini, V. Andrisano, E. Gálvez, C. Valderas, M. Unzeta, J.L. Marco-Contelles, European Journal of Medicinal Chemistry 52 (2012) 251–262.
[30] D.E. Edmonson, A. Mattevi, C. Binda, M. Li, F. Hubálek, Current Medicinal Chemistry 11 (2004) 1983–1993.
[31] T.Z.E. Jones, D. Balsa, M. Unzeta, R.R. Ramsay, Journal of Neural Transmission 114 (2007) 707–712.
[32] J. Wang, D.E. Edmonson, Biochemistry 50 (2011) 7710–7717.
[33] R.A. Scerrer, A.J. Le, Molecular Informatics 30 (2011) 386.
[34] F. Cheng, W. Li, G. Liu, Y. Tang, Current Topics in Medicinal Chemistry 13 (2013) 1273–1289.
[35] AMET Predictor, v.6.5, Simulations Plus, Inc., Lancaster, CA, 2013.
[36] ACD/Percepta 14.0.0, Advanced Chemistry Development, 2013.
[37] I. Moriguchi, S. Hirono, Q. Liu, I. Nakagome, Y. Matsushita, Chemical & Pharmaceutical Bulletin 40 (1992) 127–130.
[38] C.A. Lipinski, F. Lombardo, B.W. Dominy, P.J. Feeney, Advanced Drug Delivery Reviews 46 (2001) 3–26.
[39] H. Pajouhesh, G.R. Lenz, Drugs NeuroRx 2 (2005) 541–553.
[40] J. Kelder, P.D.J. Grootenhuis, D.M. Bayada, L.P.C. Delbressine, J.-P. Ploemen, Pharmaceutical Research 16 (1999) 1514–1519.
[41] P.A. Nielsen, O. Andersson, S.H. Hansen, K.B. Simonsen, G. Andersson, Drug Discovery Today 16 (2011) 472–475.
[42] X. Ma, C. Chen, J. Yang, Acta Pharmacologica Sinica 26 (2005) 500–512.
[43] F. Cheng, W.L. Li, Y. Zhou, J. Shen, Z. Wu, G. Liu, P.W. Lee, Y. Tang, Journal of Chemical Information and Modeling 52 (2012) 3099–3105.
[44] S. Yee, Pharmaceutical Research 14 (1997) 763–766.
[45] A. Sjöberg, M. Lutz, C. Tannergren, C. Wingolf, A. Borde, A.I. Ungell, European Journal of Pharmaceutical Sciences 48 (2013) 166–180.
[46] J.D. Irvine, L. Takahashi, K. Lockhart, J. Cheong, J.W. Tolan, H.E. Selick, J.R. Grove, Journal of Pharmaceutical Sciences 88 (1999) 28–33.
[47] S. Yamashita, T. Furubayashi, M. Kataoka, T. Sakane, H. Sezaki, H. Tokuda, European Journal of Pharmaceutical Sciences 10 (2000) 195–204.
[48] L.S. Gold, N.B. Manley, T.H. Slone, L. Rohrbach, Environmental Health Perspectives 107 (Suppl. 4) (1999) 527–600.
[49] E.J. Matthews, N.L. Kruhlak, R.D. Benz, J.F. Contreras, Current Drug Discovery Technologies 1 (2004) 61–76.
[50] L.G. Valerio Jr., K.B. Arvidson, R.F. Chanderbhan, J.F. Contrera, Toxicology and Applied Pharmacology 222 (2007) 1–16.
[51] F. Denizot, R. Lang, Journal of Immunological Methods 89 (1986) 271–277.
[52] R.A. Lenz, J.D. Baker, C. Locke, L.E. Rueter, E.G. Mohler, K. Wesnes, W. biSaab, M.D. Saltarelli, Psychopharmacology (Berl) 220 (2012) 97–107.
[53] P.J. Baarendse, G.G. Van, R.F. Jansen, A.W. Pieneman, S.O. Ogren, M. Verhage, O. Stiedl, Hippocampus 18 (2008) 11–19.
[54] G.R. Dawson, G. Bentley, F. Draper, W. Rycroft, S.D. Iversen, P.G. Pagella, Pharmacology Biochemistry and Behavior 39 (1991) 865–871.
[55] M. Grant, Journal of Comparative and Physiological Psychology 86 (1974) 853–857.
[56] R. Gupta, L.K. Gupta, P.K. Mediratta, S.K. Bhattacharya, Pharmacological Reports: PR 64 (2012) 438–444.
[57] I. Izquierdo, Trends in Pharmacological Sciences 10 (1989) 175–177.
[58] H. Sugimoto, Y. Iimura, Y. Yamanishi, K. Yamatsu, Bioorganic & Medicinal Chemistry Letters 2 (1992) 871–876.
[59] J.M. Contreras, Y.M. Rival, S. Chayer, J.-J. Bourguignon, C.G. Wermuth, Journal of Medicinal Chemistry 42 (1999) 730–741.
[60] D. Shao, C. Zou, C. Luo, X. Tang, Y. Li, Bioorganic & Medicinal Chemistry Letters 14 (2004) 4639–4642.
[61] M.I. Rodríguez-Franco, M.I. Fernández-Bachiller, C. Pérez, A. Castro, A. Martínez, Bioorganic & Medicinal Chemistry 13 (2005) 6795–6802.
[62] H. Takasugi, A. Kuno, M. Ohkubo, WO 9313083, 1993.
[63] H. Sugimoto, Y. Tsuchiya, H. Sugumi, K. Higurashi, N. Karibe, Y. Iimura, A. Sasaki, Y. Kawakami, T. Nakamura, S. Araki, Y. Yamanishi, K. Yamatsu, Journal of Medicinal Chemistry 33 (1990) 1880–1887.
[64] R. Kitbunnadaj, O.P. Zuiderveld, I.J.P. De Esch, R.C. Vollinga, R. Bakker, M. Lutz, A.L. Spek, E. Cavoy, M.-F. Deltent, W.M.P.B. Menge, H. Timmerman, R. Leurs, Journal of Medicinal Chemistry 46 (2003) 5445–5457.
[65] C.Y. Huang, Methods in Enzymology 87 (1982) 509–521.
[66] B.R. Brooks, R.E. Bruccoleri, B.D. Olafson, D.J. States, S. Swaminathan, M. Karplus, Journal of Computational Chemistry 4 (1983) 187–217.
[67] A. Morreale, F. Maseras, I. Iriepa, E. Gálvez, J. Mol, Graphics Modell 2 (2002) 111–118.